SANDIA REPORT

SAND2020-9424
Printed September 2020

Prediction of Circuit Response to an Electromagnetic Environment; ASC IC FY20 Milestone 7179

Ting Mei, Andy Huang, Heidi Thornquist, Peter Sholander and Jason Verley

Prepared by
Sandia National Laboratories
Albuquerque, New Mexico 87185
Livermore, California 94550

Issued by Sandia National Laboratories, operated for the United States Department of Energy by National Technology & Engineering Solutions of Sandia, LLC.

NOTICE: This report was prepared as an account of work sponsored by an agency of the United States Government. Neither the United States Government, nor any agency thereof, nor any of their employees, nor any of their contractors, subcontractors, or their employees, make any warranty, express or implied, or assume any legal liability or responsibility for the accuracy, completeness, or usefulness of any information, apparatus, product, or process disclosed, or represent that its use would not infringe privately owned rights. Reference herein to any specific commercial product, process, or service by trade name, trademark, manufacturer, or otherwise, does not necessarily constitute or imply its endorsement, recommendation, or favoring by the United States Government, any agency thereof, or any of their contractors or subcontractors. The views and opinions expressed herein do not necessarily state or reflect those of the United States Government, any agency thereof, or any of their contractors.

Printed in the United States of America. This report has been reproduced directly from the best available copy.

Available to DOE and DOE contractors from

U.S. Department of Energy
Office of Scientific and Technical Information
P.O. Box 62
Oak Ridge, TN 37831

Telephone: (865) 576-8401
Facsimile: (865) 576-5728
E-Mail: reports@osti.gov
Online ordering: http://www.osti.gov/scitech

Available to the public from

U.S. Department of Commerce
National Technical Information Service
5301 Shawnee Road
Alexandria, VA 22312

Telephone: (800) 553-6847
Facsimile: (703) 605-6900
E-Mail: orders@ntis.gov
Online order: https://classic.ntis.gov/help/order-methods

ABSTRACT

This report covers the work performed in support of the ASC Integrated Codes FY20 Milestone 7179. For the Milestone, Sandia's Xyce analog circuit simulator was enhanced to enable a loose coupling to Sandia's EIGER electromagnetic (EM) simulation tool. A device was added to Xyce that takes as its input network parameters (representing the impedance response) and short-circuit current induced in a wire or other element, as calculated by an EM simulator such as EIGER. Simulations were performed in EIGER and in Xyce (using Harmonic Balance analysis) for a variety of linear and nonlinear circuit problems, including various op amp circuits. Results of those simulations are presented and future work is also discussed.

EXECUTIVE SUMMARY

The overall goal of this work was to demonstrate the prediction of a nonlinear analog circuit's response when immersed in a continuous-wave (CW) electromagnetic (EM) environment. In particular, the work demonstrated the application of newly developed frequency-domain capabilities in the Xyce analog circuit simulator. It was also the first demonstration of coupling output from the EIGER frequency-domain electromagnetic simulation code to Xyce. Completion of this Milestone has resulted in a new simulation capability for the Nuclear Deterrence mission; and the work has established procedures and requirements for developing similar capabilities in the future.

Milestone Description and Completion Criteria

Milestone Description: We will demonstrate the prediction of a nonlinear analog circuit's response when immersed in a continuous-wave (CW) electromagnetic (EM) environment. This new capability will enable detailed analysis of circuit sensitivities to EM environments, including, but not limited to, weapon system circuits in hostile environments. The capability will target STS and MIL-STD frequency bands (nominally 10 kHz to tens of GHz), but will support a wide range, from DC through the GHz band. The technical approach will be to couple the EIGER frequency-domain electromagnetic simulation code to the Xyce analog circuit simulator. To enable this coupling, a new, generalized frequency-domain network parameter (S-parameter) model will be developed in Xyce.

Completion Criteria: Demonstration of the capability using an op amp circuit in an electromagnetic environment.

Grading Criteria: A program review is conducted and its results are documented. Professional documentation consisting of a report is prepared as a record of Milestone completion.

Impact Statement

A new capability has been developed for the simulation of EM effects on non-linear circuits. In addition, the effort revealed unknown limitations of the combined EIGER/Xyce toolset, which will stimulate future development. Finally, the work has established procedures and requirements for developing similar capabilities in the future.

Summary of Work Done

The initial work involved development of an “S-parameter” model in Xyce that can handle many types of network parameters, such as S (scattering), Y (admittance) and Z (impedance) parameters. To allow the input of those parameters, Xyce was enhanced to allow the reading of industry-standard Touchstone files. Also, the Touchstone standard was enhanced to allow the inclusion of short-circuit current, needed to define a complete electromagnetic response. Once the modifications were complete, they were tested against simple one- and two-port test cases created with EIGER. The EM problem involved a simple wire antenna exposed to a continuous-wave EM environment with one or both ends connected to the circuit. The circuit problem terminated the antenna with linear and/or non-linear circuit elements (resistors and diodes, specifically). The analysis was performed by importing the EM response data into Xyce and using the using the harmonic balance (HB) analysis capability. Correctness of the results was established though comparisons with analytic solutions, code-to-code comparisons, and circuit analysis techniques.

The final demonstrations of the capability involved simulations of various op amp circuits in an electromagnetic environment. Unlike the smaller test problems, the op amp low-frequency response was non-negligible. Therefore, since the EIGER code is incapable of providing DC and low-frequency response data, the missing information was calculated with the HFSS commercial EM simulator. In the test cases, the electromagnetic pickup was assumed to be on the metal circuit board traces, each one involving two ports. Up to three traces were included in the simulations for a maximum of six ports. Common commercial low- and high-bandwidth op amps were simulated for a variety of circuit responses. Comparisons were made to commercial codes, where possible, with closely matching results. The results were also analyzed analytically. The simulations showed that, even for the low-bandwidth op amp, which does not pass a high-frequency signal, a high-frequency EM wave can have a significant effect on the output.

Path Forward

As mentioned above, the successful completion of this effort has given Sandia a new simulation capability for the Nuclear Deterrence mission. In addition, the work has established procedures and requirements for developing similar capabilities in the future. The next step is to couple Xyce to Gemma, the next-generation replacement for EIGER.

ACKNOWLEDGMENTS

Much thanks to the committee members for their advice and support: Mike King, Jeff Williams, Coty Tran, Matt Young, and Brian Zinser (chair).

Also, we would like to extend thanks to the following individuals for their support. Joe Kotulski and John Himbele provided advice on the use of EIGER and gave invaluable insights on electromagnetic simulation. Isak Reines provided a physical version of an op amp circuit used in this work and associated experimental data. Shahed Reza performed the HFSS simulations, and assisted with understanding the circuit/EM simulation results. Finally, Christina Howe was the manager in charge of the work and helped with the administrative and reporting tasks.

CONTENTS

1. Introduction **11**

2. Background **12**
2.1. Xyce . . . 12
2.1.1. Circuit Theory . . . 13
2.1.2. Time Domain Simulation . . . 15
2.1.3. Frequency Domain Simulation . . . 16
2.2. EIGER . . . 19
2.2.1. Electric Field Integral Equation . . . 20
2.2.2. Method of Moments . . . 24
2.2.3. Problem specifics: wires, lumped loads, and excitation types . . . 26

3. Circuit and EM Coupling Approach **28**
3.1. Overview of the Coupling Approach . . . 28
3.2. EIGER simulations . . . 29
3.3. Xyce Frequency Domain Models . . . 30
3.3.1. S-parameter Model . . . 31
3.3.2. Active Linear Model . . . 32
3.4. Coupled Simulation Using HB . . . 32
3.4.1. Evaluating H_{HB} and the HB Jacobian . . . 33

4. Examples and Results **34**
4.1. One-port network with linear loads . . . 34
4.2. One-port network with nonlinear load . . . 36
4.3. Two-port network with nonlinear load . . . 37
4.4. Practical applications: Op Amp ICs . . . 37
4.4.1. EM coupling paths . . . 38
4.4.2. Op Amp SPICE model . . . 38
4.4.3. Calculation of DC Response . . . 39
4.5. EM Effects on 741 Op Amp . . . 40
4.5.1. EM Waves Coupled to Non-inverting Input . . . 41
4.5.2. EM Waves Coupled to Inverting Input . . . 43
4.5.3. EM Waves Coupled to Output . . . 45
4.5.4. EM Waves Coupled to All Traces . . . 46
4.6. High Bandwidth Op Amp . . . 46
4.7. Practical High Bandwidth Op Amp . . . 48

5. Conclusion **50**

References **51**

LIST OF FIGURES

Figure 2-1. Thévenin equivalent circuit 14
Figure 2-2. Norton equivalent circuit 14
Figure 2-3. Structure of the HB Jacobian matrix 18
Figure 2-4. Eiger 3D scattering problem 20
Figure 2-5. An mesh triangle element with a test point represented in barycentric coordinates, along with geometric information to define the RWG basis function. 25
Figure 2-6. Eiger wire element specification. 26
Figure 2-7. Eiger incident plane wave excitation parameterization. 27

Figure 3-1. N-port Norton equivalent circuit connected to circuit loads 28
Figure 3-2. 1-port EM problem: Y calculation (left) and I_{sc} calculation (right) 29
Figure 3-3. 1-port Norton equivalent circuit 30
Figure 3-4. 2-port EM problem: Y_{11} and Y_{21} calculation (left) and Y_{12} and Y_{22} calculation (right) 30
Figure 3-5. 2-port network 31

Figure 4-1. Magnitude of Y parameter 34
Figure 4-2. Magnitude of I_{sc} 35
Figure 4-3. Magnitude of load voltage 35
Figure 4-4. Magnitude of load voltage 36
Figure 4-5. Magnitude of load voltage in frequency domain 36
Figure 4-6. Load voltage in time domain 37
Figure 4-7. Load voltage at resistor port: frequency domain (left) and time domain (right) . 37
Figure 4-8. Load voltage at diode port: frequency domain (left) and time domain (right) . . 38
Figure 4-9. op amp circuit 39
Figure 4-10. Boyle macromodel for a BJT op amp 39
Figure 4-11. Magnitude of Y and I_{sc} for a PCB trace 40
Figure 4-12. Frequency response of 741 op amp 41
Figure 4-13. EM coupling to the non-inverting input and the resulting model 41
Figure 4-14. The induced voltage at the non-inverting input 42
Figure 4-15. DC level shift at the output due to EM disturbance 42
Figure 4-16. EM coupling to the inverting input model and the induced voltage 43
Figure 4-17. DC level shift and out-of-band high frequency AC at the output due to EM disturbance 44
Figure 4-18. EM induced voltage with a lower strength 44
Figure 4-19. The output voltage due to lower EM disturbance 45
Figure 4-20. EM coupling to the output model 45
Figure 4-21. Out-of-band high frequency AC signals at the left and right outputs 46
Figure 4-22. EM coupling to all traces model 46

Figure 4-23. Effects from EM waves coupled to all traces 47
Figure 4-24. Frequency response of high bandwidth op amp 47
Figure 4-25. The induced voltage at the non-inverting input and the effect at the output 48
Figure 4-26. The effects from EM waves coupled to all traces 48
Figure 4-27. Frequency response of LM6171 op amp 49
Figure 4-28. The induced voltage at the non-inverting input and the effect at the output 49
Figure 4-29. The effects from EM waves coupled to all traces 49

1. INTRODUCTION

The motivation of this work was to enable the prediction of a nonlinear circuit's reponse to electromagnetic (EM) environments. The EM radiation may be coupled onto internal cables and wires (which act as antennas) of an electronic system enclosure through various apertures, and induce RF voltages and currents that can be delivered to system components, such as integrated circuits. The induced voltages and currents can affect circuit performance which is analyzed in the report.

In order to predict ciruit reponse to EM enviroments, a new coupled circucit and EM simulation capability is developed. The technical approach enabling circuit and EM coupling is centered around the creation, integration, and simulation of a general frequency domain macromodel that represents the linear EM problem. In this approach, the linear EM problem is first analyzed and reduced to a Norton equivalent circuit. This Norton equivalent circuit is treated as a frequency domain macromodel in **Xyce** and connected to the nonlinear circuit loads only through defined ports. Then, the combined Norton equivalent circuit and the nonlinear circuit is solved using harmonic balance (HB) analysis. This coupling approach is general and it can be used with analytically derived, numerically simulated, or measured data.

A result of the Milestone is an exhibition of coupled frequency-domain capabilities for Xyce analog circuit simulator and **EIGER** EM simulator, and promising future directions that will address gaps in modeling and simulation needs for the ND mission. In addition, the work has established procedures and requirements for developing similar capabilities.

The rest of the report is organized as follows: Chapter 2 provides the introduction to **Xyce** and **EIGER**. This is followed by the presentation of technical approach that demonstrates the mechanisms required from both **Xyce** and **EIGER** to enable circuit and EM coupling and discussions of the individual advancements in each code in chapter 3. In chapter 4, computational results illustrate the effectiveness of the circuit and EM coupling capability that has been achieved. Additionally, the practical applications of the coupled capability to predict EM effects on multiple op amp integrated circuits are demonstrated.

2. BACKGROUND

The intent of this Milestone is to exercise newly-developed frequency-domain capabilities in the **Xyce** analog circuit simulator using an exemplar relevant to the Nuclear Deterrence (ND) mission. One of the most relevant and practical areas to exercise this capability to calculate the response of a circuit that is immersed in an electromagnetic environment. This Milestone endeavors to extend the challenge of exercising the frequency-domain capabilities in **Xyce** to coupling those capabilities with an electromagnetics code, **EIGER** (Electromagnetics Interactions GenERalized). A result of the Milestone is an exhibition of coupled frequency-domain capabilities and promising future directions that will address gaps in modeling and simulation needs for the ND mission. To allow a better understanding of the challenges of developing the frequency-domain capability in **Xyce**—in addition to the coupled capability with **EIGER**—we will present the details of both codes in the following sections.

2.1. Xyce

Xyce is a parallel analog circuit simulator [13] that is based on traditional circuit simulation tools, which were originally made popular by the Berkeley SPICE program[20]. What most distinguishes **Xyce** from SPICE is the emphasis on parallel efficiency and scalability to enable simulation of very large-scale integrated circuits (ICs). However, **Xyce** also provides non-standard device models and simulation mechanisms that enable the study of circuit response due to environmental effects, like radiation and electromagnetics. The focus on parallelism and scalability is motivated by the essential, yet expensive, need for time-domain (transient) and frequency-domain analog circuit analysis in the computer-aided design (CAD) process. The specifics of the parallel implementation and scalability of **Xyce** are not relevant to this Milestone, but can be found in various resources [14, 24, 25, 2].

Xyce was originally developed for time-domain analog circuit simulation and focused on ND-relevant circuit analysis for life extension programs (LEPs), alterations (ALTs), and surveillance. The frequency-domain analog simulation capability in **Xyce** has been recently developed due to an increasing focus on microwave and satellite applications, where radio frequency (RF) circuit analysis is more important. To support frequency-domain analysis needs, linear small signal (AC) analysis and nonlinear steady-state simulation (harmonic balance, or HB) analysis capabilities were developed. This section will provide an overview of the time-domain and frequency-domain analysis capabilities in **Xyce**, and also present some fundamental aspects of circuit theory that enable the coupling of those capabilities to an electromagnetics code.

2.1.1. Circuit Theory

Analog circuit simulation tools, like **Xyce**, are provided a list of devices along with their connectivity in an input file, often called a *netlist*. The resulting system of equations that describes this circuit network, as defined by the *netlist*, combines the device models that provide current-voltage (I-V) relationships using Kirchhoff's Current Law (KCL) and Kirchhoff's Voltage Law (KVL).

Kirchhoff's current law specifies that the sum of the branch currents into/out of any node, N_j, in the circuit must equal zero, which is expressed by

$$\sum_{i=0}^{m_j} I_i = 0, \tag{2.1}$$

where m_j is the number of branch currents, I_i, into/out of circuit node N_j. Equation (2.1) enforces the conservation of charge, as current is a measure of how much charge flows through a wire. It is also equivalent to stating that the divergence of current around a circuit node equals zero. Equation (2.1) will hold for every node in a circuit. This naturally leads to a set of coupled simultaneous equations, one for each circuit node.

Kirchhoff's voltage law (KVL) states that the sum of all the voltages around any closed loop, B_j, in a circuit must equal zero, which is expressed by

$$\sum_{i=0}^{n_j} V_i = 0, \tag{2.2}$$

where n_j is the number of branch voltages, V_i, in the closed loop, taking into account the polarities. Equation (2.2) enforces the conservation of energy, because a circuit loop is a closed conducting path, so no energy is lost. This naturally leads to another set of coupled simultaneous equations, one for each closed loop in a circuit.

Combining Kirchhoff's Current and Voltage Law can be done in a variety of ways, leading to different equation sets that represent the circuit network problem. While formulations, like Tableau, can explicitly include the full set of KCL and KVL equations, compact formulations that are more suitable for computation leverage relationships between these equation sets. An exhaustive list of these formulations, along with discussions of their strengths and weaknesses can be found in many circuit texts [3, 27, 21]. The formulation used by analog circuit simulators is a modified KCL formulation, known as Modified Nodal Analysis (MNA) [11].

Thévenin's theorem and its dual, Norton's theorem, are also commonly used for circuit analysis. These theorems are employed to simplify the study of a circuit's initial-condition and steady-state response. The equivalent circuits generated by Thévenin and Norton's theorem provide a simplification of networks made of linear time-invariant resistances, voltage sources, and current sources. In the case of this Milestone, the equivalence relationships resulting from these theorems are the key to coupling **Xyce** to the electromagnetics code, **EIGER**.

Thévenin's theorem states that *any black box containing only resistances, voltage sources and current sources can be replaced by a "Thévenin equivalent" circuit consisting of a single voltage*

source connected in series with a single resistance. As illustrated by figure (2-1), the linear network on the left in the dashed box can be replaced at terminals $A-B$ by an equivalent

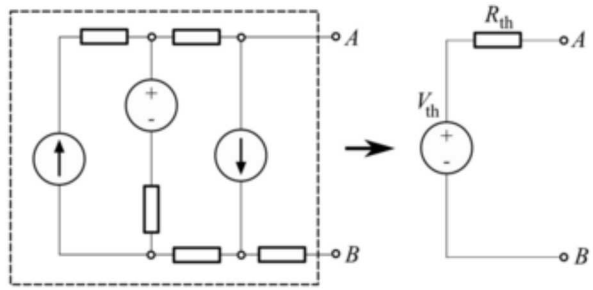

Figure 2-1. Thévenin equivalent circuit

combination of a voltage source V_{th} in a series connection with a resistance R_{th}. The equivalent voltage V_{th} is the voltage obtained at terminals $A-B$ of the network with terminals $A-B$ open circuited. The equivalent resistance R_{th} is the resistance that the circuit between terminals A and B would have if all ideal voltage sources in the circuit were replaced by a short circuit and all ideal current sources were replaced by an open circuit.

Norton's theorem states that *any black box containing only resistances, voltage sources and current sources can be replaced by a "Norton equivalent" circuit consisting of a single current source connected in parallel with a single resistance*. As illustrated by figure (2-2), the linear network on the left in the dashed box can be replaced at terminals $A-B$ by an equivalent

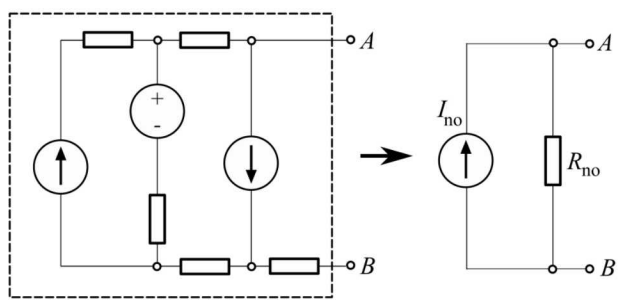

Figure 2-2. Norton equivalent circuit

combination of a current source I_{no} and a single resistor R_{no} in parallel. The equivalent current I_{no} is calculated as the current flowing at the terminals $A-B$ into a short circuit (zero resistance between A and B). The equivalent resistance R_{no} is calculated in the same way as the equivalent Thévenin resistance R_{th}.

Since they are duals, there is a simple relationship for transforming a Thévenin equivalent circuit to a Norton equivalent circuit. The equations for this transformation are simply

$$V_{th} = I_{no}R_{no}, \quad I_{no} = V_{th}/R_{th}. \tag{2.3}$$

2.1.2. Time Domain Simulation

Analog circuit simulators, like **Xyce**, combine the constitutive equations for each device (device models) using Modified Nodal Analysis to create a set of nonlinear differential algebraic equations (DAEs)

$$\frac{dq(x(t))}{dt} + f(x(t)) - b(t) = 0, \tag{2.4}$$

where $x(t) \in \mathbb{R}^n$ is the vector of circuit unknowns, $q : \mathbb{R}^n \to \mathbb{R}^n$ and $f : \mathbb{R}^n \to \mathbb{R}^n$ are functions representing the dynamic and static circuit elements (respectively), and $b(t) \in \mathbb{R}^n$ is the input vector. For many types of analysis, the initial starting point is this set of DAEs because most analog devices are defined by time-domain constitutive relationships.

Time-domain (transient) and DC (steady-state) analyses is where the set of equations (2.4), more generally expressed as

$$F(x,x') = \frac{dq(x(t))}{dt} + f(x(t)) - b(t) = 0, \tag{2.5}$$

are solved implicitly using numerical integration methods. Both analysis types require the solution to a sequence of nonlinear equations, which is typically done using Newton's method. This, in turn, results in a sequence of linear systems

$$(G + \frac{1}{\Delta t}Q)\Delta x = \frac{1}{\Delta t}(b - f) \tag{2.6}$$

involving the conductance matrix $G(t) = \frac{df}{dx}(x(t))$, and the capacitance matrix $Q(t) = \frac{dq}{dx}(x(t))$. For DC analysis, the q terms are not present in equation (2.4), so the linear system only involves the conductance matrix.

Recently, a performance improvement to the assembly of the conductance matrix $G(t)$ and capacitance matrix $C(t)$ has been made in **Xyce**. It takes advantage of the fact that device models can be separated into two groups: time-invariant (or linear) and time-variant (or nonlinear). Linear (time-invariant) devices have constitutive equations that are not time dependent and include most resistors, capacitors, inductors, and sources (voltage and current). Linear devices that are time dependent (time-varying) are considered nonlinear in this separation of devices. While the group of linear devices is small relative to nonlinear devices, they are the most common and abundantly used device models in analog circuits. Functionally, the separation of device models into two groups results in the conductance and capacitance matrix having both linear and nonlinear contributions

$$G(t) = G_{nl}(t) + G_{lin}, \;\; C(t) = C_{nl}(t) + C_{lin}. \tag{2.7}$$

For circuits that have a large number of linear devices, the separation yields a performance improvement in the time domain because G_{lin} and C_{lin} need to be assembled only once for an entire simulation. This separation of devices into different groups, and the infrastructure in **Xyce** that supports it, is leveraged and extended by this Milestone to enable more efficent simulation and coupling of frequency-domain device models.

2.1.3. Frequency Domain Simulation

Harmonic balance (HB) is a nonlinear steady-state analysis that exploits the fact that periodic waveforms can be represented by a Fourier series. The goal of HB [15] is to find the unknown Fourier coefficients of all waveforms in a circuit. To achieve this goal, the circuit equations (2.4) are written in terms of Fourier coefficients and then Newton's method is used to solve for those coefficients. Assume that both $b(t)$ and $x(t)$ are periodic with period T and $\omega_0 = \frac{2\pi}{T}$, then they can be expressed by the Fourier series

$$x(t) = \sum_{i=-\infty}^{\infty} X_i e^{ji\omega_0 t}, \;\; b(t) = \sum_{i=-\infty}^{\infty} B_i e^{ji\omega_0 t} \tag{2.8}$$

Since any function of a T-periodic signal is still periodic, $f(x(t))$ and $q(x(t))$ can be written in Fourier series

$$f(x(t)) = \sum_{i=-\infty}^{\infty} F_i(X_k) e^{ji\omega_0 t}, \;\; q(x(t)) = \sum_{i=-\infty}^{\infty} Q_i(X_k) e^{ji\omega_0 t} \tag{2.9}$$

Then, using the Fourier expansions (2.8) and (2.9), the set of equations (2.4) can be rewritten as

$$\sum_{i=-\infty}^{\infty} [ji\omega_0 Q_i(X_k) + F_i(X_k) - B_i] e^{ji\omega_0 t} = 0 \tag{2.10}$$

Since $e^{ji\omega_0 t}$ are orthogonal functions, it can be concluded that

$$ji\omega_0 Q_i(X_k) + F_i(X_k) - B_i = 0, \forall i. \tag{2.11}$$

In order to implement the harmonic balance method, it is necessary to truncate the Fourier series to a finite range, $[-M, ..., M]$. The discretized set of equations (2.11) can be written in the compact form

$$H_{HB}(X) = \Omega Q(X) + F(X) - B = 0, \tag{2.12}$$

where

$$\begin{aligned} X &= [X_{-M}, ..., X_{-1}, X_0, X_1, ..., X_M] \\ Q &= [Q_{-M}, ..., Q_{-1}, Q_0, Q_1, ..., Q_M] \\ F &= [F_{-M}, ..., F_{-1}, F_0, F_1, ..., F_M] \\ B &= [B_{-M}, ..., B_{-1}, B_0, B_1, ..., B_M] \\ \Omega &= \begin{pmatrix} -Mj\omega_0 & & \\ & \ddots & \\ & & Mj\omega_0 \end{pmatrix}. \end{aligned} \tag{2.13}$$

2.1.3.1. Evaluating H_{HB} and the HB Jacobian

The discretized equation (2.12) has implications for device models that need to be addressed in the implementation of HB. Given that the equations are in the frequency domain, the evaluation

of $Q(X)$ and $F(X)$ is also expected to be performed in the frequency domain. Most analog device models only provide consitutive equations in the time domain, so the evaluation of H_{HB} requires the discrete Fourier transform (DFT). This means that computing $Q(X)$ and $F(X)$ is a three step process:

1. Use inverse discrete Fourier transform to compute $x(t)$ from X
2. Evaluate $q(x(t))$ and $f(x(t))$
3. Use discrete Fourier transform to compute $Q(X)$ and $F(X)$ from $q(x(t))$ and $f(x(t))$, respectively

For simplicity, assume that equation (2.4) is a scalar equation and denote D and D^{-1} as the DFT and inverse DFT (IDFT) matrices, respectively. Then, the process above can be combined with equation (2.12) to give the matrix form:

$$\mathbf{H_{HB}}(X) = \Omega D\mathbb{Q}(.)D^{-1}X + D\mathbb{F}(.)D^{-1}X - B, \tag{2.14}$$

where

$$\begin{aligned} Q(X) &= D\begin{pmatrix} q(.) & & \\ & \ddots & \\ & & q(.) \end{pmatrix} D^{-1}X \\ &= D\mathbb{Q}(.)D^{-1}X \end{aligned} \tag{2.15}$$

and

$$\begin{aligned} F(X) &= D\begin{pmatrix} f(.) & & \\ & \ddots & \\ & & f(.) \end{pmatrix} D^{-1}X \\ &= D\mathbb{F}(.)D^{-1}X. \end{aligned} \tag{2.16}$$

Using Newton's method to solve $\mathbf{H_{HB}}(X) = 0$ requires a linear solve with the Jacobian matrix $\mathbf{J_{HB}} = \partial\mathbf{H_{HB}}/\partial X$ at each iteration, which is

$$\mathbf{J_{HB}} = \Omega DCD^{-1} + DGD^{-1}, \tag{2.17}$$

where

$$\begin{aligned} C &= \begin{pmatrix} C(t_0) & & \\ & \ddots & \\ & & C(t_{2M}) \end{pmatrix}, C(t_i) = \frac{dq}{dx}|_{x(t_i)} \\ G &= \begin{pmatrix} G(t_0) & & \\ & \ddots & \\ & & G(t_{2M}) \end{pmatrix}, G(t_i) = \frac{df}{dx}|_{x(t_i)}. \end{aligned} \tag{2.18}$$

2.1.3.2. HB Linear Solvers

The harmonic balance Jacobian matrix has a more complicated structure than the transient Jacobian matrix from the same circuit. The nonzero structure is necessarily related to that of the transient Jacobian matrix, as illustrated in figure 2-3, where each nonzero entry can be a dense block of size $N = 2*M+1$ [5]. Therefore, the total size of the matrix is the dimension of the

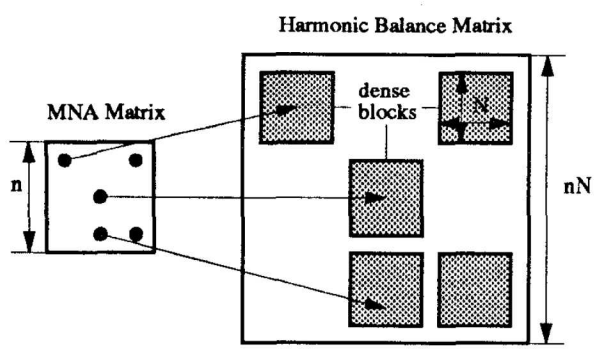

Figure 2-3. Structure of the HB Jacobian matrix

transient Jacobian multiplied by the number of harmonics, nN. For this reason, the matrix solver is the limiting factor in harmonic balance performance. The structure and size of the HB Jacobian often rules out the use of generic direct matrix solvers, although specialized direct solvers have been developed [17]. Iterative matrix solvers are the preferred solution method because they avoid the assembly and storage of the HB Jacobian, but they require an effective preconditioner [5, 18, 22, 4, 10].

Preconditioned iterative matrix solvers for harmonic balance were developed first in **Xyce**, while direct matrix solvers have been recently added. The easiest preconditioner to implement for the harmonic balance Jacobian is the block Jacobi, or averaging, preconditioner [5]. It is effective for linear through moderately nonlinear circuits and is used by default in **Xyce**. This preconditioner leverages the fact that the harmonic balance Jacobian matrix for a linear circuit is block diagonal. So, replacing the diagonals of C and G in equation (2.18) with a constant value, like the time averages

$$C_{avg} = \frac{1}{2*M+1}\sum_{i=0}^{2M} C(t_i) \quad G_{avg} = \frac{1}{2*M+1}\sum_{i=0}^{2M} G(t_i), \tag{2.19}$$

results in the matrix

$$\mathbf{J_{HBavg}} = \begin{pmatrix} -Mj\omega_0 C_{avg} + G_{avg} & & \\ & \ddots & \\ & & Mj\omega_0 C_{avg} + G_{avg} \end{pmatrix}. \tag{2.20}$$

The diagonal blocks of $\mathbf{J_{HBavg}}$ have the same sparsity pattern as the transient Jacobian, so direct matrix solvers are readily available. It is also exactly the inverse of the harmonic balance Jacobian for linear circuits, which explains its effectiveness as a preconditioner. A "corrected" (one-step) block Jacobi preconditioner is also available in **Xyce**, which uses the differences between time

averaged diagonals and the actual diagonals to improve effectiveness for more nonlinear circuits [4].

2.2. EIGER

This section includes material from the **EIGER** manual and references [29, 16]. The **EIGER** Code Suite solves electromagnetic and electro-static problems. The suite consists of five types of codes:

1. Translators that convert the output of various commercial meshing packages to a standard, minimal information, ascii-formated file known as the `*.jfg` file. A mesh can be generated in the third-party Sandia mesh generation software **CUBIT** and exported as an **Idea-s** universal `*.unv` file, which can then be converted to `*.jfg` with the **EIGER i2j** translator.

2. A pre-processor, which takes the *.jfg file and with user input determines the input needed by the physics code. This is output to an ascii formatted file known as the *.eig deck. The pre-processor is known as **Jungfrau**.

3. Two physics codes are available. **EIGER** is used to solve for the electric and magnetic currents on boundary elements when the excitation is a time-harmonic electromagnetic wave or voltage source. **Eiger_s** is used to solve for the electric charge and potential on boundary elements or volumetric elements when the excitation is a static electric field or voltage distribution. The output is written to an ascii formated file known as the *.mnh deck.

4. Two post-processors are available to obtain quantities other than the principal unknowns. They read in information from the *.eig and *.mnh decks. **Moench** is the post-processor for **EIGER**. It puts out the currents in a format that can be used in visualization software, and it computes the near and far fields at various points in space. **Moench_s** is the post-processor for **Eiger_s**. It puts out the charge and potential in a format that can be used in visualization software and it computes the near electric fields.

5. Translators that convert the output of various codes in the **EIGER** Code Suite to a format that can be read by commercial packages. Two examples are: EigerVTK, which converts the file generated by **Moench** into a file that can be rendered by ParaView and **j2i**, which converts a `*.jfg` file generated by **i2j** or by **Jungfrau** into a universal file understood by the meshing package **Idea-s**.

The subject of the present report leverages the **EIGER** electromagnetic dynamic simulation tool to simulate induced current on an electrically conducting object. The problem set-up involves generating a geometry mesh (e.g., using **CUBIT** and translated using the **i2j** tool), running the pre-processing tool **Jungfrau** which provides a series of prompts for describing the physical problem and creates an `*.eig` input deck. Finally, **EIGER** is run on the eig input deck, and produces the output mnh file.

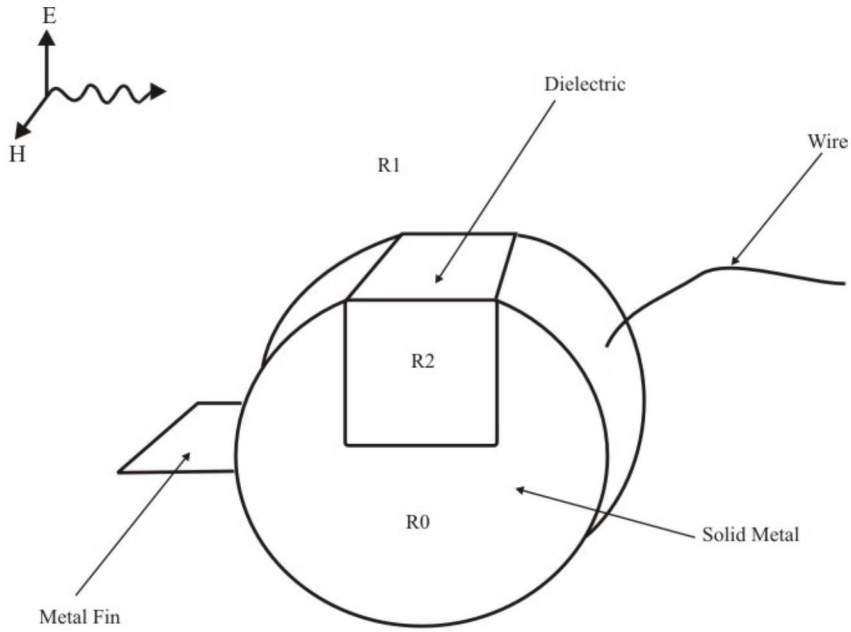

Figure 2-4. Eiger 3D scattering problem

The 3d scattering problem consists of a plane wave incident on a scattering object as shown in Figure 2-4. In **EIGER** the 3d scattering geometry is defined by a set of surfaces that divide space into volumes. These volumes are known in **EIGER** as “regions". In the Figure 2-4, R0 is a metal region, R1 is the free-space region that surrounds the scattering object and extends to infinity and R2 is a dielectric region. Note that the region id “0" is reserved in **EIGER** to represent metal – perfect electrical conductor (PEC) or perfect magnetic conductor (PMC). The remaining region ids (in this case 1 and 2) identify regions other than metal and need to eventually be defined by the user when setting up the problem in **Jungfrau**.

Also supported are special mesh elements - metal fins and wires - which do not divide space in regions. Lumped load elements are also available, and can be used to represent a resistor. For this report, all electromagnetic geometries analyzed by **EIGER** were constructed using wire mesh elements and lumped loads. This is not a restriction on the presented coupling formulation whatsoever, but simplified mesh generation.

2.2.1. Electric Field Integral Equation

EIGER simulates the radiated electric field due to the induced surface current by an external excitation - for example, a voltage source or an incident electromagnetic wave. In this section, we briefly review the electromagnetic theory necessary to describe the Electric Field Integral Equation (EFIE) numerically solved by an **EIGER** simulation. We adopt the following notation

for the quantities:

$$\begin{aligned}
\vec{B} &\equiv \text{magnetic flux density } [Vs/m^2] \\
\vec{H} &\equiv \text{magnetic field intensity } [A/m] \\
\vec{D} &\equiv \text{electric flux density } [C/m^2] \\
\vec{E} &\equiv \text{electric field intensity } [V/m] \\
\varepsilon &= \text{permittivity } [F/m] \\
\varepsilon_0 &= \text{vacuum permittivity} = 8.83 \times 10^{-12}\,[F/m] \\
\varepsilon_r &= \text{relative permittivity } [1] \\
\mu &= \text{permeability } [H/m] \\
\mu_0 &= \text{free space permeability} = 4\pi \times 10^{-7}\,[H/m] \\
\mu_r &= \text{relative permeability } [1]
\end{aligned}$$

Their constitutive relations are:

$$\vec{B} = \mu \vec{H} \tag{2.21}$$

$$\vec{D} = \varepsilon \vec{E} \tag{2.22}$$

$$\varepsilon = \varepsilon_r \varepsilon_0 \tag{2.23}$$

$$\mu = \mu_r \mu_0 \tag{2.24}$$

The point of departure is the set of Maxwell's equations governing the coupled electromagnetic fields:

$$\text{Gauss' law: } \nabla \cdot \vec{D} = \rho \tag{2.25}$$

$$\text{Gauss' law for magnetism: } \nabla \cdot \vec{B} = 0 \tag{2.26}$$

$$\text{Maxwell-Faraday equation: } \nabla \times \vec{E} = -\frac{\partial \vec{B}}{\partial t} - \vec{M}^i \tag{2.27}$$

$$\text{Ampère's law: } \nabla \times \vec{H} = \frac{\partial \vec{D}}{\partial t} + \vec{J}^i + \vec{J}^d \tag{2.28}$$

EIGER solves a derived form of Maxwell's equations. We now begin a derivation of an expression which directly relates $\vec{E}$ to $\vec{J}^i$. Appearing on the right-hand sides of the immediately preceding equations are the quantities:

$$\begin{aligned}
\vec{M}^i &\equiv \text{impressed (source) magnetic current density } [V/m^2] \\
\vec{J}^i &\equiv \text{impressed (source) electric current density } [A/m^2] \\
\vec{J}^d &\equiv \text{electric displacement current density } [A/m^2]
\end{aligned}$$

We remark that the terms $\vec{J}^c := \frac{\partial \vec{D}}{\partial t}$ and $\vec{M}^d := -\frac{\partial \vec{B}}{\partial t}$ are the electric conduction current density $[A/m^2]$ and the magnetic displacement current density $[V/m^2]$, respectively. For the circuit coupling problem, we will consider the case in which $\vec{M}^i = \vec{0}$. We also have the expression $\vec{J}^d = \sigma \vec{E}$, where σ is the surface charge density $[A/m^2]$.

In the frequency domain, equations (2.27) and (2.28) become

$$\nabla \times \vec{E} = -j\omega\vec{B}$$
$$\nabla \times \vec{H} = j\omega\varepsilon\vec{E} + \vec{J}^i + \sigma\vec{E}$$

where ω is a given frequency; these equations equate the $e^{j\omega t}$ coefficients in the Fourier series expansion. We identify the complex electric permittivity as the coefficient

$$\hat{\varepsilon} := \varepsilon_0 \left(\varepsilon_r - \frac{j\sigma}{\omega\varepsilon_0} \right)$$

and finally re-express these equations as

$$\nabla \times \vec{E} = -j\omega\vec{B} \tag{2.29}$$
$$\nabla \times \vec{H} = j\omega\hat{\varepsilon}\vec{E} + \vec{J}^i \tag{2.30}$$

2.2.1.1. Potential formulation

There exists a vector potential $\vec{A}$ for which

$$\vec{B} = \nabla \times \vec{A} \tag{2.31}$$

since $\vec{B}$ is divergence-free by (2.26). In the frequency domain, (2.27) and (2.31) yield

$$\nabla \times \left(\vec{E} + j\omega\vec{A} \right) = 0. \tag{2.32}$$

This field is irrotational and so there exists a potential Φ for which

$$\vec{E} = -j\omega\vec{A} - \nabla\Phi \tag{2.33}$$

Restricting to a surface between regions, we have the continuity equation

$$\nabla_\Sigma \cdot \vec{J}_\Sigma = -j\omega\sigma \tag{2.34}$$

Consider the quantity $\nabla \times \nabla \times \vec{A}$. By equations (2.31) and (2.30), we have

$$\begin{aligned} \nabla \times \nabla \times A &= \nabla \times \vec{B} \\ &= \nabla \times \left(\mu\vec{H} \right) \\ &= \mu\nabla \times \vec{H} \\ &= \mu j\omega\hat{\varepsilon}\vec{E} + \mu\vec{J}^i \end{aligned} \tag{2.35}$$

Substituting for $\vec{E}$ according to equation (2.33), we arrive at

$$\nabla \times \nabla \times \vec{A} = \mu j\omega\hat{\varepsilon} \left(-j\omega\vec{A} - \nabla\Phi \right) + \mu\vec{J}^i \tag{2.36}$$

Applying the vector identity

$$\nabla \times \nabla \times \vec{A} = \nabla \left(\nabla \cdot \vec{A} \right) - \nabla^2 \vec{A}, \tag{2.37}$$

to equation (2.36) implies

$$\nabla \left(\nabla \cdot \vec{A} \right) - \nabla^2 \vec{A} = \mu j \omega \hat{\varepsilon} \left(-j\omega \vec{A} - \nabla \Phi \right) + \mu \vec{J}^i \tag{2.38}$$

Choosing the Lorenz gauge yields

$$\begin{aligned} \nabla \cdot \vec{A} &= -j\omega \hat{\varepsilon} \mu \Phi \\ \Rightarrow \nabla \left(\nabla \cdot \vec{A} \right) &= -j\omega \hat{\varepsilon} \mu \nabla \Phi \end{aligned} \tag{2.39}$$

This reduces equation (2.38) to a Helmholtz equation for $\vec{A}$:

$$\begin{aligned} -\nabla^2 \vec{A} &= \mu \omega^2 \hat{\varepsilon} \vec{A} + \vec{J}^i \\ \Rightarrow -\left(\nabla^2 + \mu \omega^2 \hat{\varepsilon} \right) \vec{A} &= \vec{J}^i \end{aligned} \tag{2.40}$$

We consider $k := \sqrt{\mu \omega^2 \hat{\varepsilon}}$ the wave number in the equation. The self-adjoint elliptic operator $\mathscr{L} \equiv -(\nabla^2 + k^2)$ admits a Green's function G which satisfies

$$\mathscr{L}(x) G(x,s) = \delta(x-s)$$

in the sense of distributions, where the right-hand side is the Dirac delta distribution. For any sufficiently smooth function $f(x)$ vanishing on the boundary of a domain D, we have

$$\int_D \mathscr{L}(x) G(x,s) f(x)\, dx = \int \delta(x-s) f(x)\, dx = f(s).$$

This is useful because we can deduce an expression for $\vec{A}$ in terms of $\vec{J}^i$:

$$\mathscr{L}(x) \vec{A}(x) = \vec{J}^i(x) \tag{2.41}$$

$$\Rightarrow \int_D \left(\mathscr{L}(x) \vec{A}(x) \right) G(x,x') dx' = \int_D \vec{J}^i(x) G(x,x') dx' \tag{2.42}$$

$$\Rightarrow \int_D \vec{A}(x) \left(\mathscr{L}(x) G(x,x') \right) dx' = \int_D \vec{J}^i(x') G(x,x') dx' \tag{2.43}$$

$$\Rightarrow \int_D \vec{A}(x) \delta(x-x') dx' = \int_D \vec{J}^i(x') G(x,x') dx' \tag{2.44}$$

The preceding equations were obtained successively by: multiplying by G and integrating over D with respect to x', using self-adjointness of $\mathscr{L}$ on the left-hand side and integrating the right-hand-side by parts, and applying the identity $\mathscr{L} G = \delta$. Hence, we arrive at the formula for the vector potential:

$$\boxed{\vec{A}(\vec{x}) = \mu \iiint_V G\left(\vec{x}, \vec{x'}\right) \vec{J}^i(\vec{x'})\, d\vec{x'}} \tag{2.45}$$

for a closed volume V. Applying $\nabla\cdot$ to equation (2.40), we see that

$$-(\nabla^2+k^2)(-j\omega\hat{\varepsilon}\mu\Phi) = \mu\nabla\cdot\vec{J}^i$$
$$\Rightarrow -(\nabla^2+k^2)\Phi = \frac{1}{-j\omega\hat{\varepsilon}}\nabla\cdot\vec{J}^i$$

At this point, we may make use of the continuity equation (2.34) to obtain

$$-(\nabla^2+k^2)\Phi = \frac{\rho^i}{\hat{\varepsilon}}, \tag{2.46}$$

the wave equation for the scalar potential. Using the Green's function method, we find that

$$\boxed{\Phi(\vec{x}) = \frac{1}{-j\omega\hat{\varepsilon}}\iiint_V G\left(\vec{x},\vec{x'}\right)\nabla\cdot\vec{J}^i(\vec{x'})\,d\vec{x'}} \tag{2.47}$$

Combining equations (2.45) and (2.47) in the expression (2.33), we arrive at the electric field integral equations (EFIE):

$$\boxed{\begin{aligned}\vec{n}\times\vec{E}^{inc} = &-j\omega\mu\vec{n}\times\iiint_V G\left(\vec{x},\vec{x'}\right)\vec{J}^i(\vec{x'})\,d\vec{x'}\\ &-\vec{n}\times\nabla\left[\frac{1}{-j\omega\hat{\varepsilon}}\iiint_V G\left(\vec{x},\vec{x'}\right)\nabla\cdot\vec{J}^i(\vec{x'})\,d\vec{x'}\right]\end{aligned}} \tag{2.48}$$

Thus, given an incident electric field $\vec{E}^{inc}$, the EFIE can be used to solve for the surface current $\vec{J}^i$. Note that the induced current $\vec{J}^i$ is supported on the boundary surfaces between regions. The following section details a numerical procedure to solve for that induced current.

2.2.2. Method of Moments

In order to numerically solve (2.48) for the current $\vec{J}$, we can adopt a solution ansatz by choosing a basis of functions for vector fields on the surfaces between regions. The mesh of surfaces by triangular elements allows the use of Rao-Wilton-Glisson (RWG) basis functions. On any given triangular mesh element, these are defined as following. The test point is at $\vec{r}$ and can be expressed in barycentric coordinates, $(\xi_{\beta-1},\xi_\beta,\xi_{\beta+1})$. Addtionally, the $\vec{h}$'s are "height vectors", $\vec{e}$'s are "edge vectors" and $\vec{v}$'s are "vertex vectors". Additionally, a normal vector, $\hat{n}$, is defined to be a unit vector orthogonal to the edge vectors. From this geometric information on the supporting triangles, we can define the basis function:

$$\vec{\Lambda}_\beta(\vec{r}) = \frac{\vec{r}-\vec{v}_\beta}{h_\beta} \tag{2.49}$$
$$= \frac{\vec{e}_{\beta-1}\xi_{\beta+1}-\vec{e}_{\beta+1}\xi_{\beta-1}}{h_\beta} \tag{2.50}$$

Each basis function is associated to an edge of the triangular mesh, and is only non-zero on the two triangular mesh elements that share that edge. The standard RWG basis function maintains

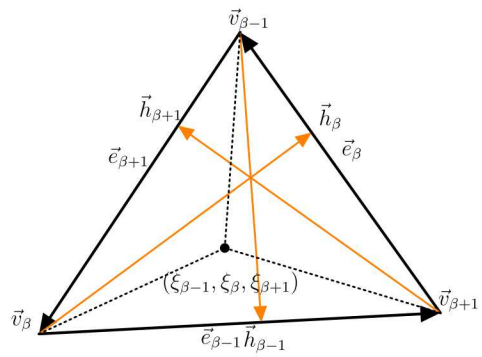

Figure 2-5. An mesh triangle element with a test point represented in barycentric coordinates, along with geometric information to define the RWG basis function.

unit normal continuity (meaning the normal component of the vector basis is constant) across the edge and has zero normal component to the other edges of the elements.

Now, in order to numerically solve the EFIE equation, **EIGER** enumerates all n edges of the triangular mesh and represents the current as $\vec{J}(\vec{r}) = \sum_{i=1}^{n} J_i \vec{\Lambda}_i(\vec{r})$. Then, the EFIE equation is solved weakly: by testing against the basis function $\vec{\Lambda}_k$, we obtain:

$$\begin{aligned}\sum_{i=1}^{n} J_i \Bigg[j\omega\mu \int_{S_k}\int_{S_i} \vec{\Lambda}_k(\vec{r}) \cdot \vec{\Lambda}_i(\vec{r}') G(\vec{r},\vec{r}')\, ds_i\, ds_k - \\ \int_{S_k} \left(\nabla \cdot \vec{\Lambda}_k \frac{1}{-j\omega\hat{\varepsilon}} \int_{S_i} G(\vec{r},\vec{r}') \nabla_{S_i} \vec{\Lambda}_i(\vec{r}')\, ds_i \right) ds_k \Bigg] \\ = \int_{S_k} \vec{\Lambda}_k(\vec{r}) \cdot \vec{E}^{inc}_{tan}(\vec{r})\, ds_k \, \forall k\end{aligned} \tag{2.51}$$

Denote the matrix appearing on the right hand side by

$$\begin{aligned}Z_{ik} = j\omega\mu \int_{S_k}\int_{S_i} \vec{\Lambda}_k(\vec{r}) \cdot \vec{\Lambda}_i(\vec{r}') G(\vec{r},\vec{r}')\, ds_i\, ds_k - \\ \int_{S_k} \left(\nabla \cdot \vec{\Lambda}_k \frac{1}{-j\omega\hat{\varepsilon}} \int_{S_i} G(\vec{r},\vec{r}') \nabla_{S_i} \vec{\Lambda}_i(\vec{r}')\, ds_i \right) ds_k\end{aligned} \tag{2.52}$$

called the Method of Moments impedance matrix. Denoting by $\vec{V}$ the vector with entries

$$V_k = \int_{S_k} \vec{\Lambda}_k(\vec{r}) \cdot \vec{E}^{inc}_{tan}(\vec{r})\, ds_k \tag{2.53}$$

and applying some numerical quadrature scheme to all integrals (care must be given to the numerical treatment of the singularity in the Green's function), we arrive at the dense $n \times n$ linear system

$$\mathbf{Z}\vec{I} = \vec{V} \tag{2.54}$$

Finally, we remark that in **EIGER**, the surfaces are the entities that are gridded not the regions. The regions surrounding each surface are tagged referring to the surface normals. The surfaces

can represent solid metal, which divide the region outside the metal region from region 0 (the default metal region id). The surfaces can represent a dielectric, which divide an outside dielectric region from an inside dielectric region. Metal surfaces with the same region on both sides are called metal fins in **EIGER**. A metal fin designation invokes EFIE equations and have unknowns that represent total current on both sides of the fin. Wires are modeled using bar elements, which are the naturally defined lower-dimensional realization of the RWG basis functions (all coinciding with the Raviert-Thomas basis functions for edge and triangular meshes).

2.2.3. Problem specifics: wires, lumped loads, and excitation types

As described in the preceding sections, the mesh of a geometric structure is required for electromagnetic dynamic simulation. For the coupling problems studied in this report, these structures are geometrically describable by 1-dimensional segments. A straight wire and the traces of the circuit board are two such examples. See Figure 2-6 for a diagram of the relationship between RWG basis functions and wire elements defined over two adjacent edges. The RWG basis function b1 is supported on the two mesh triangles e3 and e9, whereas the wire element b4 is defined on the bar elements e5 and e7; it has a positive gradient along the e5 edge (oriented from node p10 to node p5) and has a negative gradient along the e7 edge (oriented from node p5 to node p17). On such a wire basis element, **EIGER** can prescribe a lumped load (resistor) across

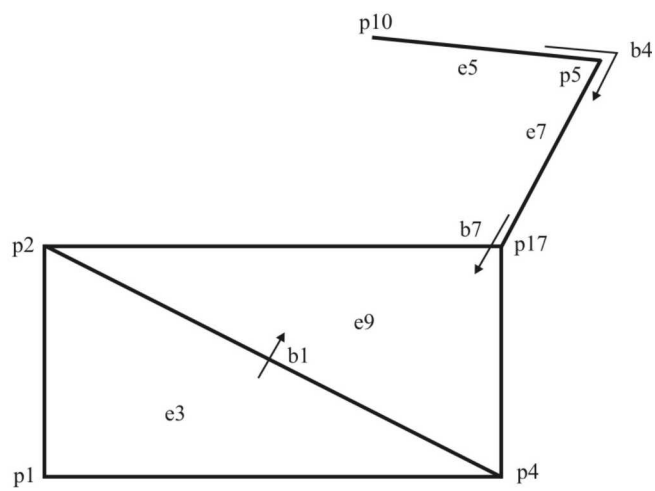

Figure 2-6. Eiger wire element specification.

a bar element or provide a point voltage excitation across the bar element. Note that some care must be given to the prescription of the lumped load or the voltage excitation in order to respect the orientation of the basis function and to remain consistent with the voltage drop direction (e..g, from node p5 to node p17, rather than the other way, etc.). This kind of point voltage-dependent source takes the form

$$V = -I_n Z_L L_n \tag{2.55}$$

where n corresponds to the basis element index, L_n corresponds to the bar element length, and I_n is the current on the nth element. And so, a lumped load is accounted for in the numerical

treatment by a modification of the impedance matrix; where Z is the original impedance matrix, the addition of a lumped load takes the form:

$$Z_{with\,load} = Z + (L_n)^2 Z_L \delta_{mn} \tag{2.56}$$

The other kind of electromagnetic excitation relevant to our coupling problem is a plane wave excitation. The plane wave characteristics are shown in Figure 2-7 below. Note that the plane wave is defined with the head of the propagation vector pointing at the origin. Note that θ is the angle with respect the $+z$ axis and ϕ is the angle that the projection of the propagation vector on the xy plane makes with the x axis. H_θ is the H field along the θ direction. H_ϕ is the H field along the ϕ direction. The H field of the plane wave is defined at the origin in terms of a complex quantity in units of amps/meter.

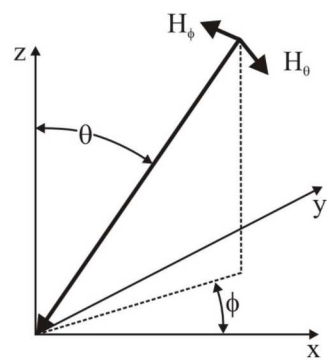

Figure 2-7. Eiger incident plane wave excitation parameterization.

3. CIRCUIT AND EM COUPLING APPROACH

This section will build on the introduction to **Xyce** and **EIGER**, provided in chapter 2, to explain the technical approach taken and contributions achieved by this Milestone. First, an overview of the technical approach will be presented that illustrates the mechanisms required from both **Xyce** and **EIGER** to enable circuit and EM coupling. This will be followed by discussions of the individual advancements in each code that was motivated by the technical approach. In chapter 4, computational results will illustrate the effectiveness of the circuit and EM coupling capability that has been achieved by this Milestone.

3.1. Overview of the Coupling Approach

The technical approach enabling circuit and EM coupling is centered around the creation, integration, and simulation of a general frequency domain macromodel that represents the linear EM problem. In this approach, the linear EM problem is first analyzed and reduced to a Norton equivalent circuit. This Norton equivalent circuit is treated as a frequency domain macromodel in **Xyce**, and is connected to the nonlinear circuit loads only through defined ports, as shown in figure 3-1. Then, the combined Norton equivalent circuit and the nonlinear circuit is solved using harmonic balance (HB) analysis. This coupling approach is general, and it can be used with analytically derived, numerically simulated, or measured data. It is comparable to the ATHENA [28] model, and the approaches used in [23, 12, 19, 26].

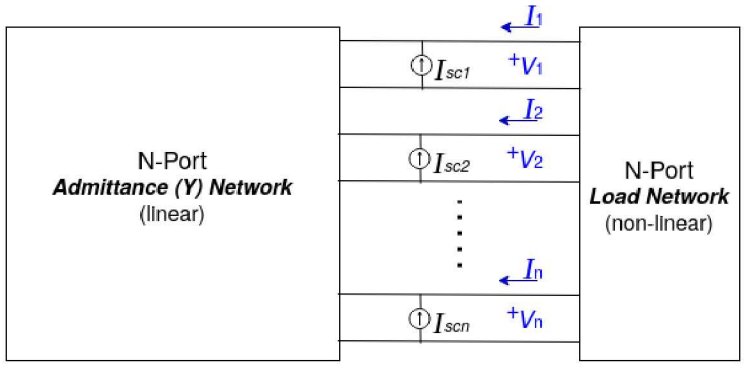

Figure 3-1. N**-port Norton equivalent circuit connected to circuit loads**

Norton's theorem, as discussed in chapter 2, provides the theoretical foundation for creating an equivalent circuit that can be used to replace a network of resistors and sources. The linearity of

the EM problem allows it to be represented by a multi-port Norton equivalent circuit, where the port currents and voltages are described by the following equation:

$$I = YV - I_{sc}. \tag{3.1}$$

Given N number of ports, I, V, and I_{sc} are vectors of length N for the port currents, voltages, and short-circuit current sources, respectively. The admittance matrix for the EM system, Y, is $N \times N$. All of these parameters are frequency dependent. While the linear EM problem can also be represented by a Thévenin equivalent circuit, the Norton equivalent circuit is more compatible with the modified nodal analysis (MNA) formulation used in **Xyce** [11].

Constructing the Norton equivalent circuit for a linear EM problem requires Y and I_{sc}. These parameters can be obtained using any time-domain or frequency-domain EM simulator or analysis technique. Furthermore, the linear EM problem is only solved once for each frequency, which means it can be efficiently computed prior to the **Xyce** HB analysis.

3.2. EIGER simulations

For this Milestone, **EIGER** is the frequency domain EM simulator used to solve the linear EM problem. It does not provide the parameters to define the Norton equivalent circuit directly, so a two-step approach has been developed in order to determine Y and I_{sc}. This approach is demonstrated for a 1-port EM problem in figure 3-2, where both the positive and negative nodes for the single port are explicitly shown. In the first step, a 1 V AC voltage source is applied to the

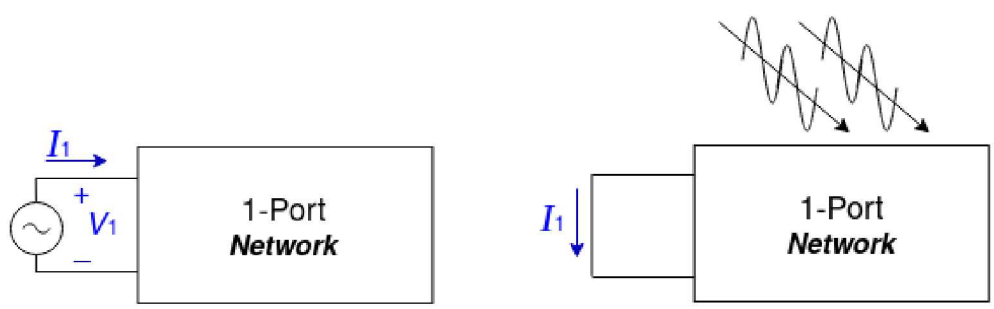

Figure 3-2. 1-port EM problem: Y calculation (left) and I_{sc} calculation (right)

port. **EIGER** calculates the induced current throughout the entire geometry. Then, some post-processing (by identifying the port geometrically on the object) is performed to obtain the current at the port. This gives the Y parameter. In the second step, an incident plane wave excitation is applied to the body and the port is short-circuited. Again, EIGER determines the induced current throughout the entire geometry, and from this the port current is obtained, yielding the I_{sc} parameter. The resulting Norton equivalent circuit that represents this 1-port EM problem is shown in figure 3-3.

This two-step approach has been generalized to analyze and reduce a N-port EM problem. For a N-port problem, the Y parameter is a $N \times N$ matrix and I_{sc} is a vector of length N. In the first step, N simulations are needed to compute the admittance matrix, one for each column of Y. To do

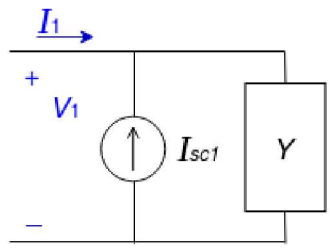

Figure 3-3. 1-port Norton equivalent circuit

that, each port is excited with a 1 V voltage source in sequence with all other ports short circuited. The currents at all the ports are calculated by **EIGER**, which produces one column of Y. The 2-port EM problem in figure 3-4 demonstrates the approach for calculating the elements of Y:

$$Y = \begin{pmatrix} Y_{11} & Y_{12} \\ Y_{21} & Y_{22} \end{pmatrix}.$$

In the second step, an incident electric field is applied with all ports short circuited and **EIGER** is used to compute the currents at all the ports, which gives the I_{sc}. In general, for a N-port EM problem, $N+1$ simulations are necessary to compute the Norton equivalent circuit.

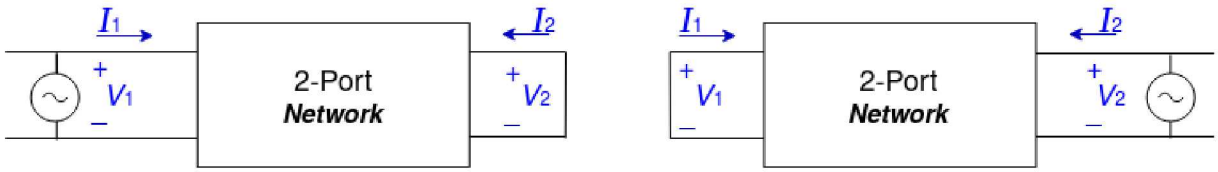

Figure 3-4. 2-port EM problem: Y_{11} and Y_{21} calculation (left) and Y_{12} and Y_{22} calculation (right)

3.3. Xyce Frequency Domain Models

The set of transient DAE equations (2.4) needs to be extended to include frequency-domain models that do not have a constitutive (I-V) relationship. This results in

$$\int_{-\infty}^{t} y(t-s)x(s)ds + \frac{dq(x(t))}{dt} + f(x(t)) - b(t) = 0, \tag{3.2}$$

where y represents the matrix-valued impulse response function of frequency-domain linear elements (such as S parameters). Prior to the separation of devices models into multiple groups, as discussed in chapter 2, frequency-domain models needed to implement this convolution operation to be usable in **Xyce**. This was the case for the original implementation of the ATHENA model [28]. In the frequency domain, the convolution in equation (3.2) is naturally replaced by a matrix multiplication, which motivates the extension of device model groups to include linear frequency-domain models. This section will present the general multi-port, active linear frequency-domain macromodel developed in **Xyce** that enabled coupling to the **EIGER** electromagnetics code. This will include a detailed discussion of the two types of linear frequency-domain macromodels: passive and active.

3.3.1. S-parameter Model

The passive linear frequency-domain model is normally referred to as the S-parameter model. It is available in many modern commercial simulators, and is widely used by RF and microwave design communities. The S-parameter model has a standard input-output (I/O) format and therefore is portable among simulators. Developed in support of this Milestone, the S-parameter model in **Xyce** can handle many types of network parameters, such as S (scattering), Y (admittance) and Z (impedance) parameters.

This device model has a frequency-domain I-V relationship at the ports represented by the Y parameters:

$$I = YV \tag{3.3}$$

For a N-port linear network, I and V are vectors of length N for the port currents and voltages, respectively. The admittance matrix, Y, is $N \times N$. Figure 3-5 shows a two-port network, where the following equations define the Y parameters

$$Y_{11} = \left.\frac{I_1}{V_1}\right|_{V_2=0} \quad Y_{21} = \left.\frac{I_2}{V_1}\right|_{V_2=0} \quad Y_{12} = \left.\frac{I_1}{V_2}\right|_{V_1=0} \quad Y_{22} = \left.\frac{I_2}{V_2}\right|_{V_1=0} \tag{3.4}$$

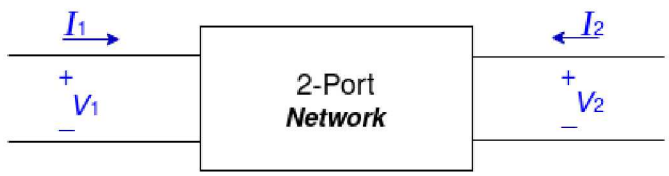

Figure 3-5. 2-port network

Some network parameters, such as scattering parameters, do not provide an I-V relationship. Therefore, it is necessary to convert them to other network parameters that provide a frequency-domain I-V relationship to enable their use in a circuit simulator. The scattering parameters and admittance parameters satisfy the following relationship

$$Y = G_{rs}(E - S)(E + S)^{-1} G_{rs}, \tag{3.5}$$

where Y is the $N \times N$ admittance matrix, S is the $N \times N$ scattering matrix, and E is the $N \times N$ identity matrix. G_{rs} is defined as:

$$G_{rs} = \begin{pmatrix} G_1 & & & \\ & G_2 & & \\ & & \ddots & \\ & & & G_N \end{pmatrix}, \quad G_i = \frac{1}{\sqrt{Re|Z_i|}}, \tag{3.6}$$

where Z_i is the reference impedance of port i. Impedance (Z) parameters can be converted to admittance parameters using the following simple formula

$$Y = Z^{-1}.$$

3.3.2. Active Linear Model

The technical approach presented in this Milestone to enable circuit and EM coupling requires an active, linear frequency domain macromodel to include the incident EM fields that are represented by short-circuit current sources. To achieve this, a general frequency domain macromodel was developed in **Xyce** that can be used as both a passive S-parameter model—using an industrial standard I/O definition—and an active model (Norton or Thévenin equivalent circuit). The active model extends the S-parameter model to include short-circuit current sources. Therefore, it supports multiple types of network parameters, including S, Y and Z parameters. This approach also makes it possible to use measured data, which is beneficial because voltage and current are difficult to measure at high frequencies. Scattering (S) parameters are widely used to characterize a linear network especially by designers of high frequency circuits. In order to work with a variety of data, including the measured data, interpolation was also developed for the general frequency domain macromodel.

3.4. Coupled Simulation Using HB

The previous sections discussed the technical approach for creating a Norton equivalent circuit for the linear EM problem with **EIGER**, and using that circuit as an active, linear frequency domain macromodel in **Xyce**. This section will present the approach for performing a coupled simulation that produces the circuit response to an EM environment. This coupled simulation is achieved using the harmonic balance (HB) analysis, provided by **Xyce**, extended to include linear frequency-domain device models.

Frequency domain HB analysis solves for steady state solutions for nonlinear circuits. One of the main strengths of HB is its natural support for linear frequency-domain models, making it a natural choice for coupled simulation. Distributed components—such as lossy transmission lines and interpolated tables of S-parameters—are examples of linear models that are handled efficiently with HB, as is the active, linear frequency domain macromodel developed in this Milestone.

The derivation of the HB equations, including the residual equation and Jacobian, as well as the matrix solution methods, are presented in chapter 2. Including linear frequency-domain models into those equations is mathematically straightforward, because the convolution integral in the first term of equation (3.2) is replaced by a matrix multiplication. So, replacing all the transient terms with Fourier expansions, equation (2.10) becomes

$$\sum_{i=-\infty}^{\infty} [Y_i X_i + j\omega_i Q_i(X_k) + F_i(X_k) - B_i] e^{j\omega_i t} = 0. \tag{3.7}$$

Since $e^{j\omega_i t}$ are orthogonal functions, equation (2.11) becomes

$$Y_i X_i + j\omega_i Q_i(X_k) + F_i(X_k) - B_i = 0, \forall i. \tag{3.8}$$

The HB equation system can be writen in a compact form using a truncated Fourier series in a finite range: $[-M,...,M]$

$$H_{HB}(X) = YX + \Omega Q(X) + F(X) - B = 0, \tag{3.9}$$

where Y is the admittance matrix for the frequency-domain devices and all other matrices are defined in equation (2.13).

3.4.1. Evaluating H_{HB} and the HB Jacobian

The evaluation of H_{HB} primarily requires the evaluation of $Q(X)$ and $F(X)$ using the discrete Fourier transform, but there is now an additional step for the admittance matrix Y.

1. Use inverse discrete Fourier transform to compute $x(t)$ from X
2. Evaluate $q(x(t))$ and $f(x(t))$
3. Use discrete Fourier transform to compute $Q(X)$ and $F(X)$ from $q(x(t))$ and $f(x(t))$, respectively
4. Compute YX

For simplicity, assume that equation (3.2) is a scalar equation and denote D and D^{-1} as the DFT and IDFT matrices, respectively. Then, the process above can be combined with equation (3.9) to give the matrix form:

$$\mathbf{H_{HB}}(X) = YX + \Omega D\mathbb{Q}(.)D^{-1}X + D\mathbb{F}(.)D^{-1}X - B, \tag{3.10}$$

where $\mathbb{Q}$ and $\mathbb{F}$ are defined by equations (2.15) and (2.16), respectively. The active, linear frequency domain macromodel developed in this Milestone contributes to both $F(X)$ and B in the HB residual equation (3.10). The contribution of I_{sc} is included in B. Using Newton's method to solve $\mathbf{H_{HB}}(X) = 0$ requires a linear solve with the Jacobian matrix $\mathbf{J_{HB}} = \partial \mathbf{H_{HB}}/\partial X$ at each iteration, which is

$$\mathbf{J_{HB}} = Y + \Omega DCD^{-1} + DGD^{-1}, \tag{3.11}$$

where C and G are defined by equation (2.18).

4. EXAMPLES AND RESULTS

In this chapter, a variety of examples are presented to illustrate the effectiveness of the coupled circuit and EM capability. The capability is verified in multiple ways for both linear and nonlinear circuit problems. All the test cases presented here support the technical approach enabling circuit and EM coupling that culminates in the simulation of a general frequency domain macromodel that represents the linear EM problem using the harmonic balance algorithm in Xyce.

4.1. One-port network with linear loads

The EM problem is a one meter wire excited by incident electrical field. It is solved by **EIGER** and then reduced to a one-port Norton equivalent circuit. The frequency spectrum is calculated from 10 MHz to 600 MHz with a step of 10 MHz. The calculated Y and I_{sc} are shown in figures 4-1 and 4-2.

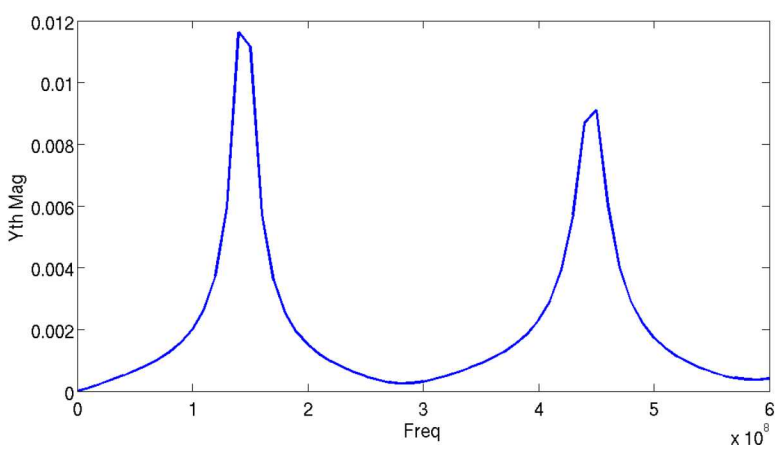

Figure 4-1. Magnitude of Y parameter

The load for the port is a 50 Ω resistor. The port voltage, as simulated in **Xyce**, is shown in figure 4-3. Since the load is linear, the combined EM and linear load simulation can also be completed by **EIGER**. The **EIGER** result is is also shown in figure 4-3. As can be seen, the Xyce HB result and the **EIGER** result match well.

Because the problem is linear, the port voltage can be calculated analytically using

$$V = \frac{I_{sc}}{Y_{tot}} \tag{4.1}$$

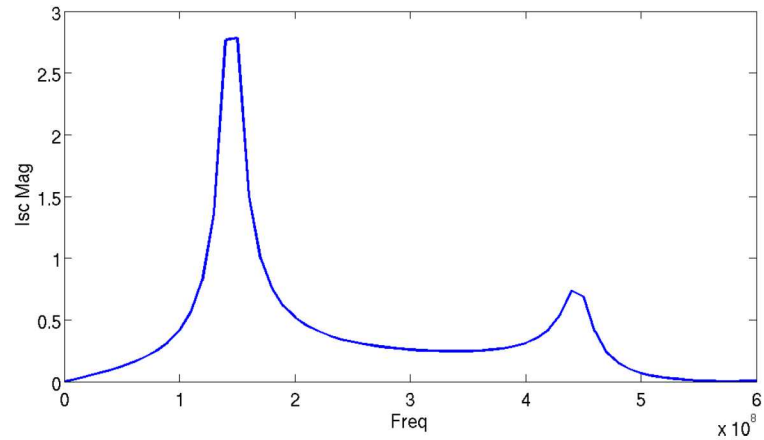

Figure 4-2. Magnitude of I_{sc}

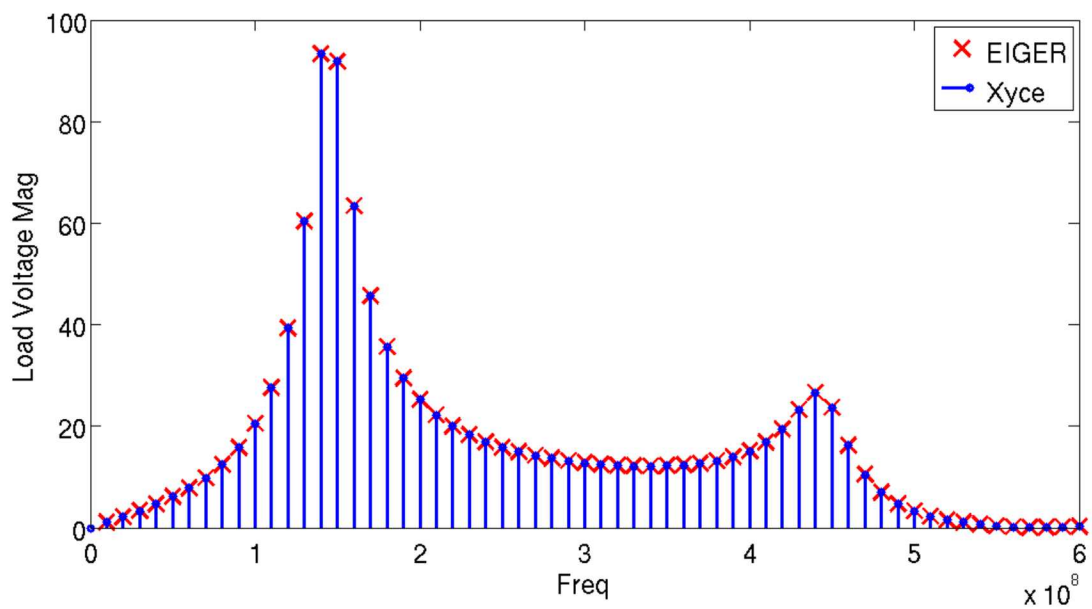

Figure 4-3. Magnitude of load voltage

Here Y_{tot} is the total admittance, and is defined as:

$$Y_{tot} = Y + \frac{1}{R_L} \tag{4.2}$$

The total admittance is dominated by the conductance of the load resistor, because it is much larger than Y. Therefore, the shape of port voltage in figure 4-3 is similar to that of I_{sc}.

With a linear load of 1000 Ω, the conductance of the load is comparable to Y. The port voltages solved by coupled simulation in **Xyce** and by **EIGER** are shown in figure 4-4. Again, the **Xyce** HB result and **EIGER** result match well.

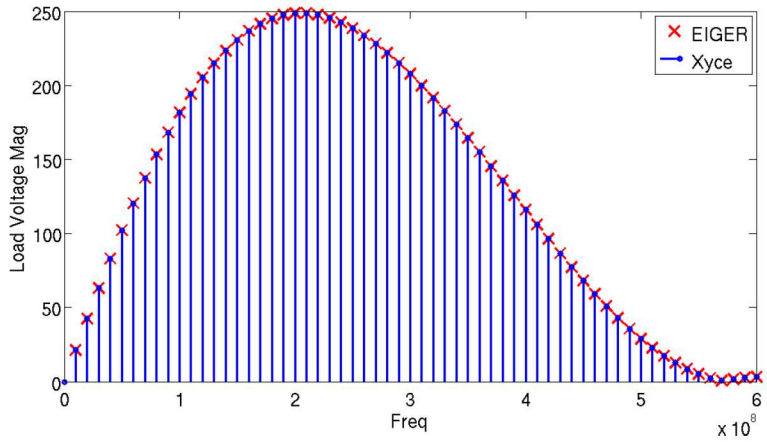

Figure 4-4. Magnitude of load voltage

4.2. One-port network with nonlinear load

The EM problem is, again, a one meter wire excited by incident electrical field. For the nonlinear load, a diode is placed in parallel with the 50 Ω resistor. The wire is excited with a 10 MHz plane wave. The port voltage, solved by coupled simulation in **Xyce**, is shown in figures 4-5 and 4-6. **EIGER** simulation cannot be used for verification, because it cannot handle nonlinear devices. As a check of the result, the **Xyce** simulation is compared against Hspice RF by using a combination of HB, S-parameter model and frequency domain sources in Hspice. The **Xyce** HB results and Hspice results match well.

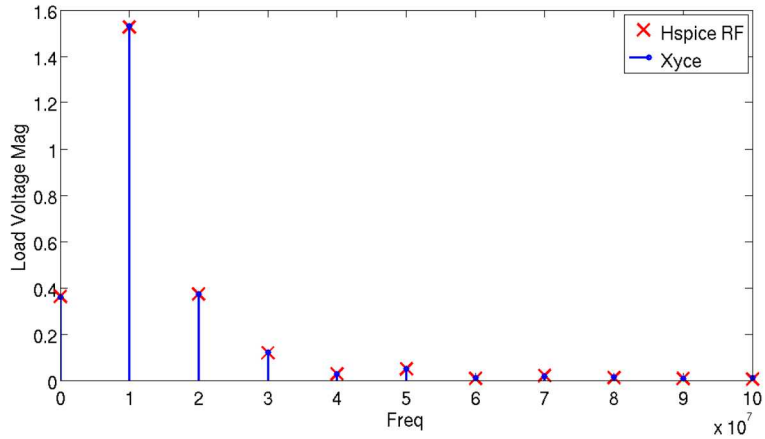

Figure 4-5. Magnitude of load voltage in frequency domain

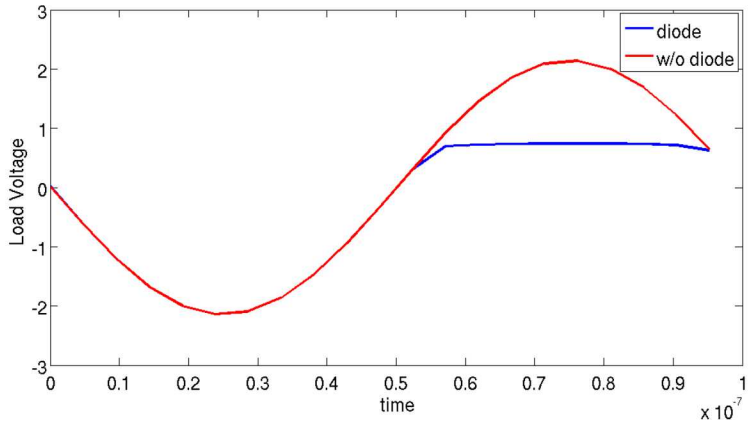

Figure 4-6. Load voltage in time domain

4.3. Two-port network with nonlinear load

The same EM problem can also be used as a two-port network with a port at each end of the wire. In this example, one port is loaded with a 50 Ω resistor. The other port is loaded with a diode. The voltage at the port with a resistor, solved by coupled simulation in **Xyce**, is shown in figure 4-7. As expected, the port voltage is a sinusoidal waveform with same frequency as the excitation. To verify the results, the time-domain **Xyce** results are compared against Hspice RF results. The two results match well.

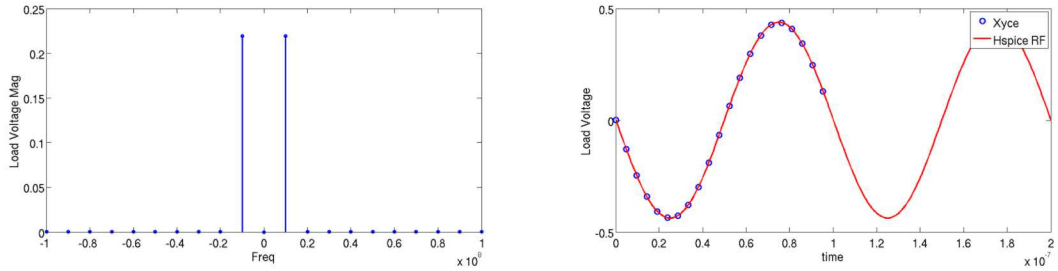

Figure 4-7. Load voltage at resistor port: frequency domain (left) and time domain (right)

The voltage at the diode port, solved by coupled simulation in **Xyce**, is shown in figure 4-8. We note that the DC level is shifted. The behavior is similar to a clamper circuit. The wire behaves like a capacitor which provides DC offset from stored charge. Again, the time-domain **Xyce** results are compared against Hspice RF results, and the two results match well.

4.4. Practical applications: Op Amp ICs

In the next few sections, the coupled circuit and EM capability is applied to practical circuits, such as operational amplifiers, to investigate the EM effects on circuits.

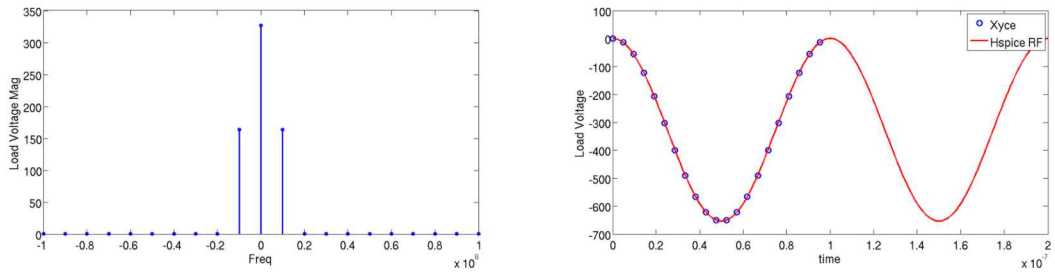

Figure 4-8. Load voltage at diode port: frequency domain (left) and time domain (right)

4.4.1. EM coupling paths

Operational amplifiers (op amps) are a fundamental building blocks that are used widely in circuit design. In order to predict a circuit's response to EM environments, a model is needed to identify the possible coupling paths from the EM-induced signals to op amps. Then we can apply the coupled simulation to study the interaction between received signal at the pins of op amp and op amp circuit.

There are two different types of coupling paths: radiation and conduction. When each one comes into play depends on the frequency of the EM waves and susceptibility of each circuit element at that frequency. The radiation coupling path means the op amp ICs, themselves, pick up the EM waves. For the conduction path, other devices, such as cables and printed circuit board (PCB) traces, act as receiving antenna for the EM waves. For the frequency range of interest (100 MHz to 1 GHz), the dimensions of a typical op amp are small compared to the wavelength of the disturbing EM signals. Therefore, the disturbing EM waves mainly arrive in a conductive way. It is sufficient to consider only the conductively received EM waves.

The op amp circuits used for this work are configured as differential op amps, as shown in figure 4-9, with a closed-loop gain of 3. Currents are induced on the PCB traces by the EM disturbances and are conducted to the pins of the op amps. They can interfere with op amp operation. For this example, the EM disturbance is considered to be confined to the three traces that are connected to the non-inverting and inverting input pins and the output pin of the op amp. This is because these are the EM disturbances that are the most difficult to prevent [6, 7].

4.4.2. Op Amp SPICE model

To simulate the combined EM and op amp circuit problem in **Xyce**, a model for the op amp is needed. One of the most widely used op amp simulation models is a modified version of the Boyle macromodel [9]. The Boyle macromodel does not simulate the internal circuitry at the device level. Instead, it uses macromodeling to represent amplifier behavior as observed at the terminals. The circuit schematic for the Boyle macromodel of a bipolar op amp is shown in figure 4-10. The model consists of three connected stages: the input stage, the intermediate voltage gain stage and the output stage.

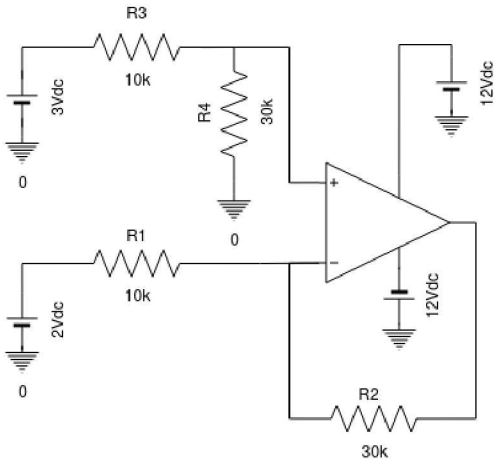

Figure 4-9. op amp circuit

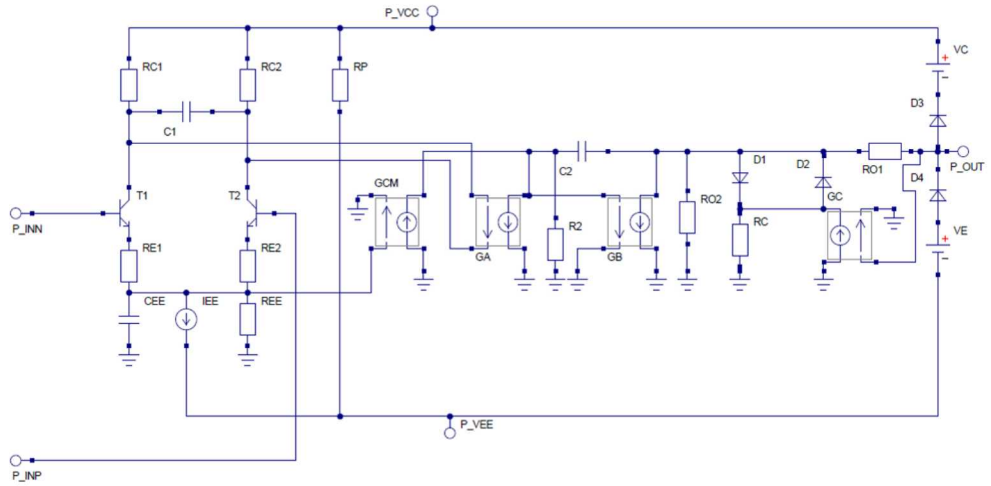

Figure 4-10. Boyle macromodel for a BJT op amp

The modified Boyle macromodel was orignially developed for use with the PSpice circuit simulator [1]. The models provided by many semiconductor manufacturers are based on the modified Boyle macromodel. They have the same netlist structure as the one is PSpice. However, the parameters for the device components can be different.

4.4.3. Calculation of DC Response

Harmonic balance simulation requires device data at frequencies that are integer multiples of the fundamental frequency, including at DC. The EM problem is solved by **EIGER** and is represented by a frequency domain macromodel which requires Y and I_{sc}. A PCB trace exposed to EM waves can be represented by a two port network. The calculated Y and I_{sc} from **EIGER** are shown in figure 4-11.

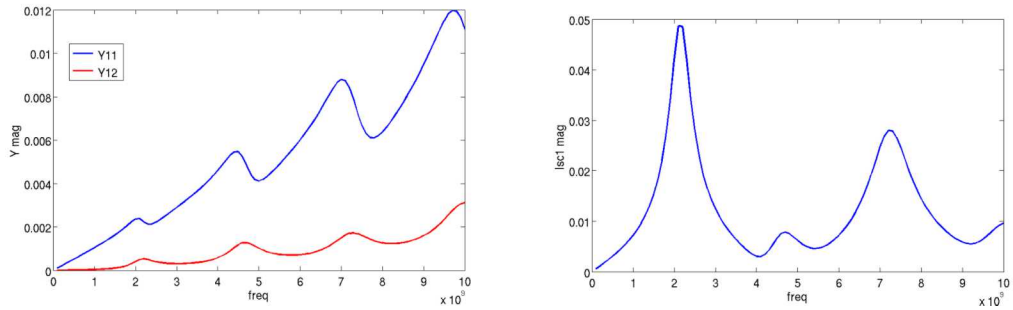

Figure 4-11. Magnitude of Y and I_{sc} for a PCB trace

A problem with the **EIGER** simulation is that no DC data can be provided. If the Y parameters are extrapolated to get the DC data, they are virtually zeros, indicating the trace does not conduct signal at DC. This is inconsistent with the physics. A trace is designed to conduct signal at DC and this is confirmed by measurements. To address this issue, a hybrid model is developed for the PCB trace. The Y parameters at high frequencies are calculated by **EIGER** and the DC response is calculated using a different analysis.

The PCB trace behaves like a resistor at DC. The resistance can be calculated according to the trace dimensions, temperature, and material (copper) using equation 4.3.

$$R = \rho \cdot \frac{L}{T \cdot W} \cdot [1 + \alpha \cdot (temp - 25)] \tag{4.3}$$

Here ρ is resistivity. L, T, W are the length, thickness, and width of a trace, respectively. The Y parameters can be derived from calculated trace resistance. For the traces on the op amp PCB, the dimensions are: $W = 60$ mil and $T = 7$ mil. The lengths are approximately two inches. For example, for a 2 inch trace, the Y parameters are:

$$Y = \begin{pmatrix} G & -G \\ -G & G \end{pmatrix}, \quad G = \frac{1}{R} = 313.5$$

The calculated Y parameters match those from HFSS which is a commercial EM simulator.

4.5. EM Effects on 741 Op Amp

The UA741 op amp is one of the most common commercial circuits. It has 1 MHz unity gain bandwidth and a slew rate of 0.5 V/μs. The internal frequency compensation ensures stability.

The frequency response of UA741 op amp, configured as in figure 4-9, is simulated using Xyce AC analysis. The result is shown in figure 4-12. As can be seen, it has a closed-loop gain of 3 at DC. The gain decreases at higher frequencies and is virtually zero at frequencies larger than 100 MHz. The bandwidth is about 300 kHz. The op amp PCB is excited by a 1 GHz plane wave. Therefore, the EM disturbances are mostly outside the working bandwidth. The effects from each input and output trace, as well as the total effects from all traces, are investigated using coupled simulations.

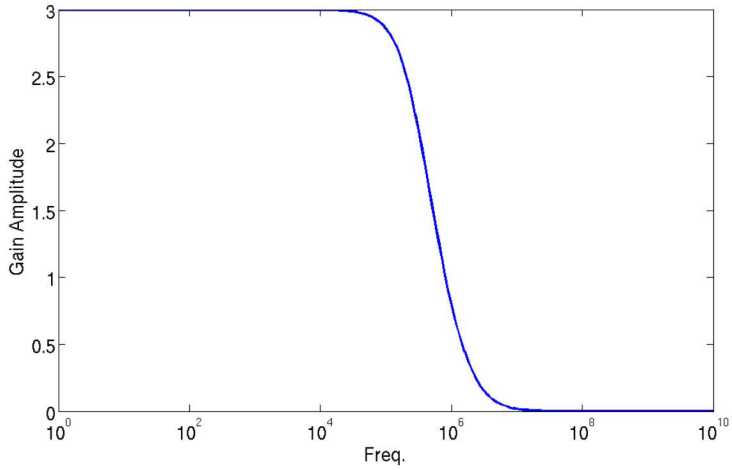

Figure 4-12. Frequency response of 741 op amp

4.5.1. EM Waves Coupled to Non-inverting Input

In this example, the EM wave is coupled to the non-inverting input trace and then is conducted to the input pin of the op amp. The EM coupling process, and the resulting model used in the simulation, are shown in figure 4-13.

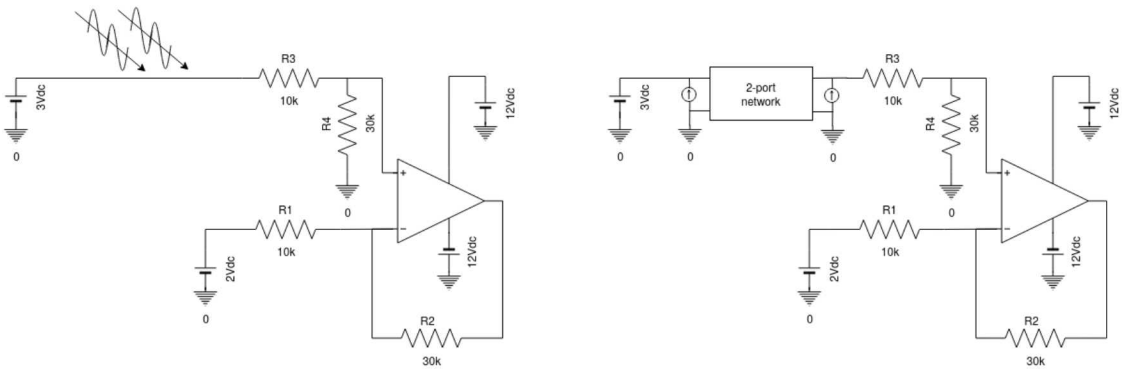

Figure 4-13. EM coupling to the non-inverting input and the resulting model

Since the op amp is configured as a differential voltage amplifier, the EM effect on the circuit depends on the induced voltage at the non-inverting input pin. As can be seen in the figure 4-13, the EM induced voltage depends not only on Y and I_{sc} from the EM calculation, but also on the impedance of the op amp at the non-inverting input. The induced voltage at the non-inverting input is shown in figure 4-14. The peak to peak voltage is about 10.5 V.

The output voltage due to the EM disturbance on the non-inverting input is shown in figure 4-15. As can be seen, the out-of-band EM disturbance leads to a DC level shift at the output. The shift is about 130 mV, which is significant and can cause problems in subsequent circuits.

To verify this result, the **Xyce** HB result is compared to Hspice RF HB results. As shown, the two results match well. In addition, a convergence study is done to verify the Xyce result. It requires

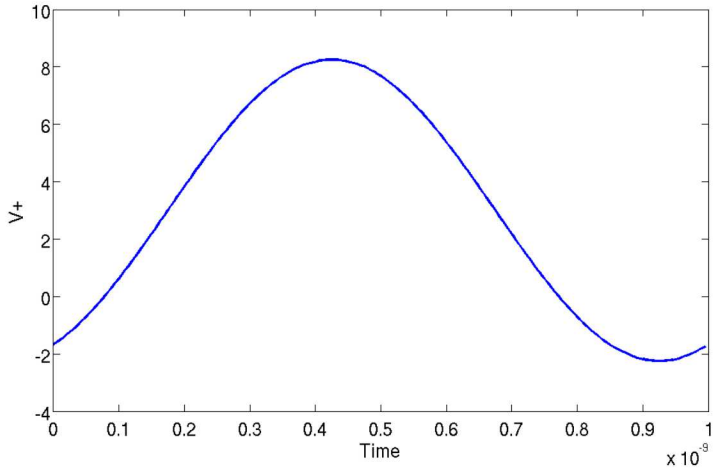

Figure 4-14. The induced voltage at the non-inverting input

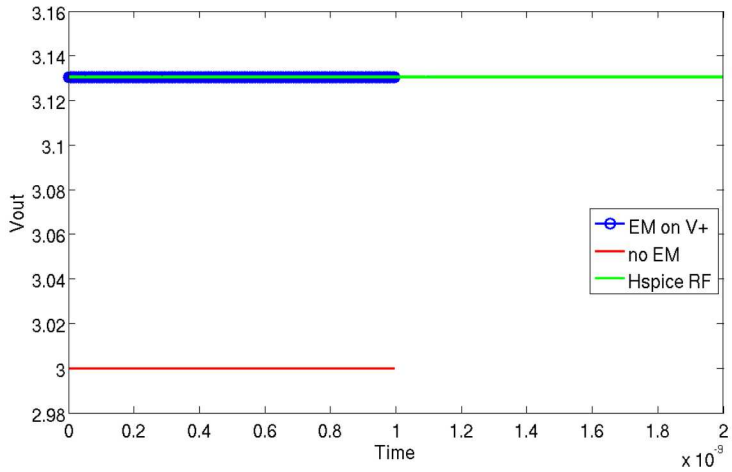

Figure 4-15. DC level shift at the output due to EM disturbance

almost 100 harmonics for the result to converge. The EM interacts with op amps via the nonlinearity of the op amp circuit. The highest nonlinearity is obtained for the disturbance with a frequency that is outside the band of op amp circuit. Therefore, a large number of harmonics are needed to calculate the correct results.

The EM induced output DC level shift in an op amp has been investigated both theoretically and experimentally in the literature [6, 7, 8]. The behavior is correlated to slew rate asymmetry and the unequal parasitic capacitances. Investigation of the behavior can provide guidance in the design phase to improve EM performance.

4.5.2. EM Waves Coupled to Inverting Input

In this example, the inverting input trace is excited by 1 GHz plane wave. The circuit, including the EM coupling model, along with the induced voltage at the inverting input are shown in figure 4-16. The peak-to-peak voltage is about 10.5 V.

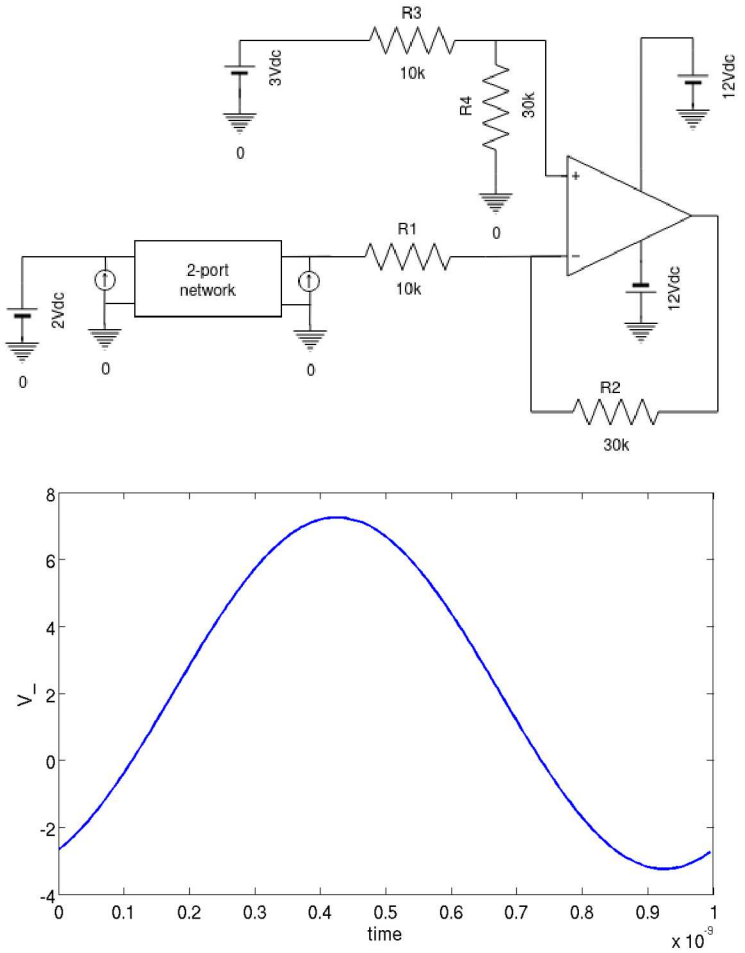

Figure 4-16. EM coupling to the inverting input model and the induced voltage

The output voltage due to the EM disturbance on the inverting input is shown in figure 4-17. As can be seen, the out-of-band EM disturbance leads to both a negative DC level shift and out-of-band high frequency AC signals at the output. The DC shift is about -171 mV. The high frequency signals are due to the feedback loop in the op amp.

The result is compared to existing measurements from a combined environment study. The standard measurement method, Direct Power Injection (DPI), is used in the study. In DPI, the EM disturbance is modeled as sinusoidal waveform and is injected to the pin of an IC. In this case, the measured data is obtained by injecting a 1 GHz RF signal into the inverting input. The strength is about 20 dBm, which corresponds to an approximately 10.5 V peak to peak voltage. The measured DC shift is about -300 mV. The Xyce simulation result qualitatively matches the

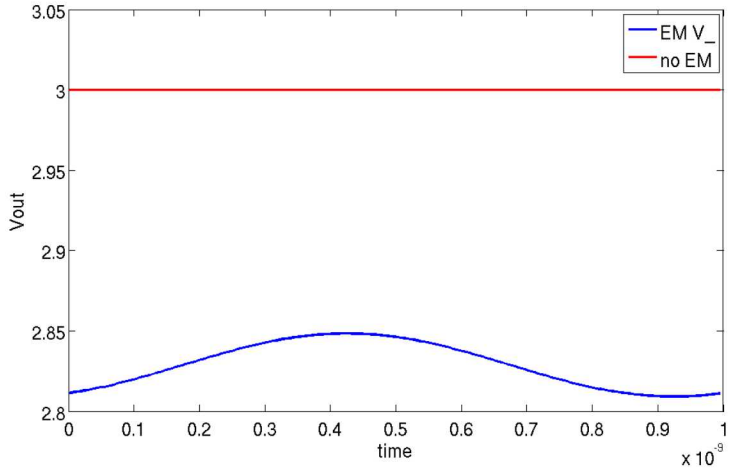

Figure 4-17. DC level shift and out-of-band high frequency AC at the output due to EM disturbance

measured data. The standard macromodel models the standard op amp performance and is not adequate to predict second order effects in op amp slew rate. In order to accurately predict the DC shift induced by an out-of-band EM disturbance, an EMI oriented op amp macromodel is needed [6].

Figure 4-18 shows the induced voltage at the inverting input with a low strength EM wave. The peak to peak voltage is about 2.9 V.

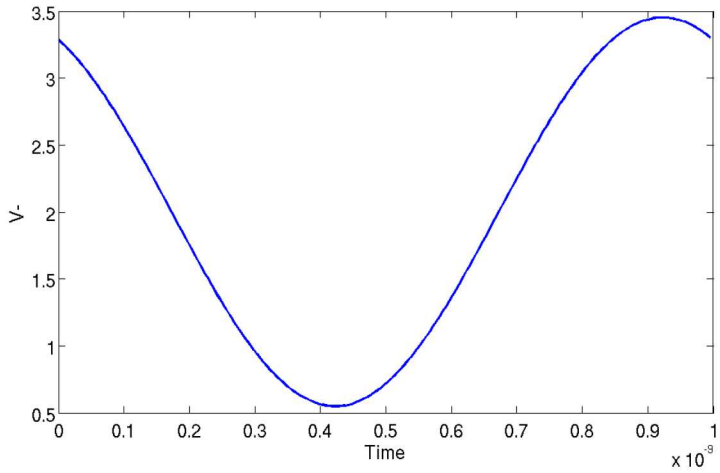

Figure 4-18. EM induced voltage with a lower strength

The output voltage due to the EM disturbance on the inverting input is shown in figure 4-19. As shown, the out-of-band EM disturbance leads to a much smaller negative DC level shift at the output. The DC shift is about -16 mV. As can be seen from the comparison with the previous result, there is a nonlinear relationship between the strength of the induced voltage and the DC shift.

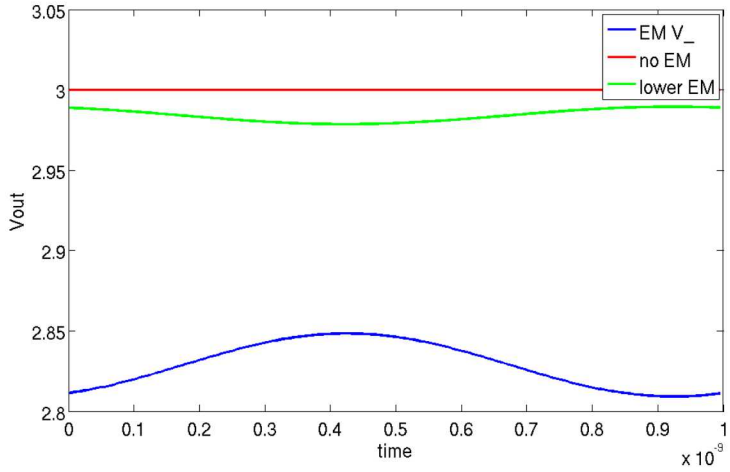

Figure 4-19. The output voltage due to lower EM disturbance

4.5.3. EM Waves Coupled to Output

In this example, the output trace is excited by a 1 GHz plane wave. The circuit with the EM coupling model is shown in figure 4-20. The output voltages at both left and right ports due to the

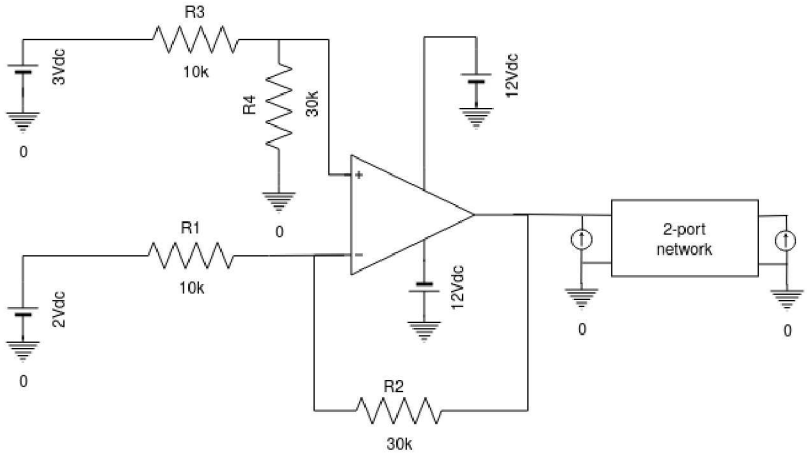

Figure 4-20. EM coupling to the output model

EM disturbance on the output trace are shown in figure 4-21. As can be seen, the EM disturbance leads to out-of-band high frequency AC signals at the outputs. The EM induced voltage at the left port has a smaller amplitude because the output impedance of the op amp is small. At the right port, the op amp has an open load. Therefore, the induced voltage depends only on the Y and I_{sc}.

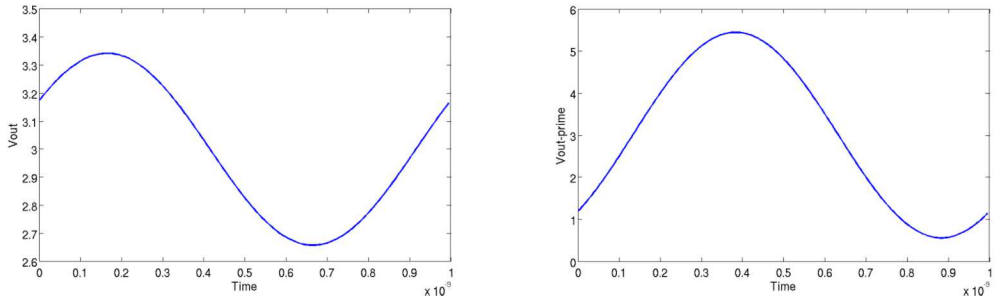

Figure 4-21. Out-of-band high frequency AC signals at the left and right outputs

4.5.4. EM Waves Coupled to All Traces

In this example, all traces are excited by a 1 GHz plane wave from the direction $\theta = 30°$ and $\phi = 60°$. The circuit along with the EM coupling model is shown in figure 4-22.

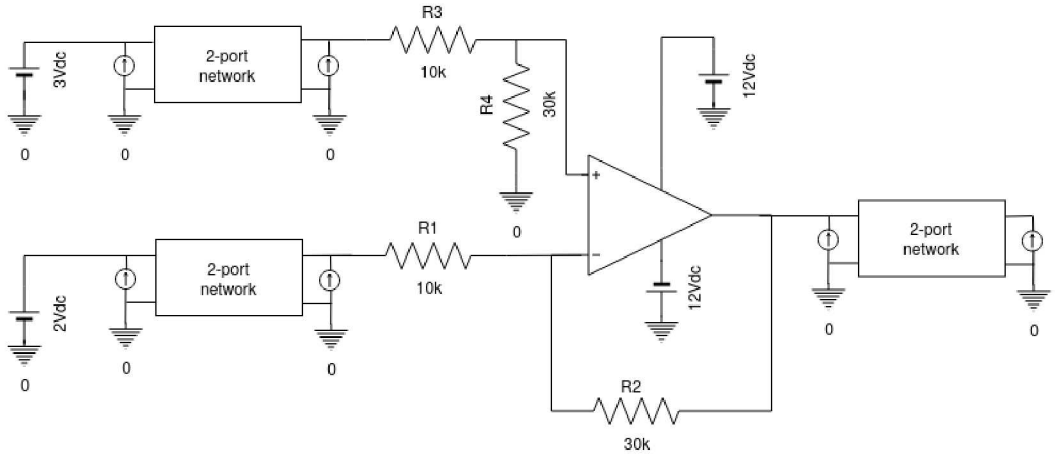

Figure 4-22. EM coupling to all traces model

The output voltage due to the EM disturbance on all traces is shown in figure 4-23. As can be seen, the EM effect is the combination of the previous results with both a DC level shift and out-of-band high frequency AC signals at the output.

4.6. High Bandwidth Op Amp

The 741 op amp is internally compensated, which limits bandwidth. This is modeled by the feedback capacitor C2 in the Boyle macromodel, shown in figure 4-10. Modifying C2 can lead to a bandwidth change, which is the same compensation modification often used by designers. In this example, a high bandwidth op amp is obtained by reducing C2. The frequency response is shown in figure 4-24. As can be seen, it has a bandwidth of about 300 MHz. The op amp PCB is excited by a 1 GHz plane wave. Therefore, EM disturbances are close to the working bandwidth.

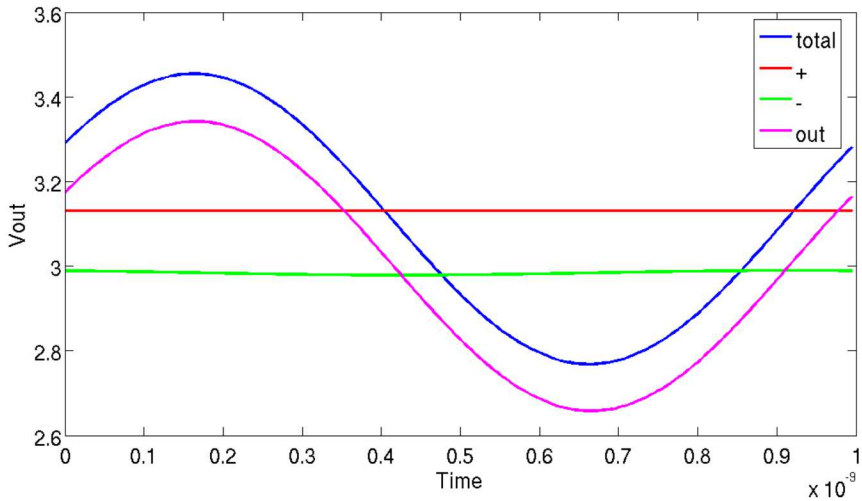

Figure 4-23. Effects from EM waves coupled to all traces

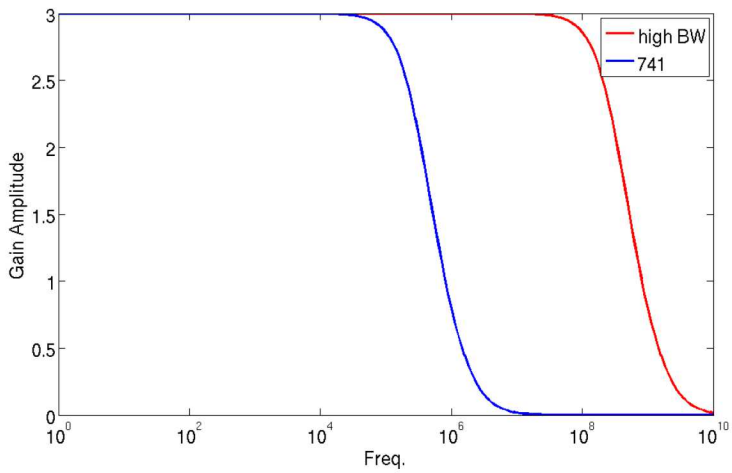

Figure 4-24. Frequency response of high bandwidth op amp

In the first example, the EM wave is coupled to the non-inverting input trace and then is conducted to the input pin of the op amp. The induced voltage at the non-inverting input and the effect at the output are shown in figure 4-25. The peak to peak voltage at input is about 2.1 V. The in-band EM leads to distorted AC signal at the output. This is due to slew rate limiting.

The output voltage due to the EM disturbance on all traces is shown in figure 4-26. All traces are excited by a 1 GHz plane wave from the direction $\theta = 30°$ and $\phi = 60°$. As can be seen, the EM effect is the combination of effects from each trace, resulting in a distorted high frequency AC at the output.

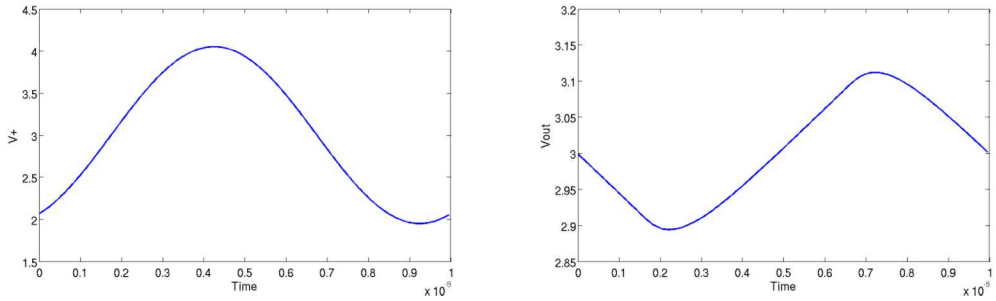

Figure 4-25. The induced voltage at the non-inverting input and the effect at the output

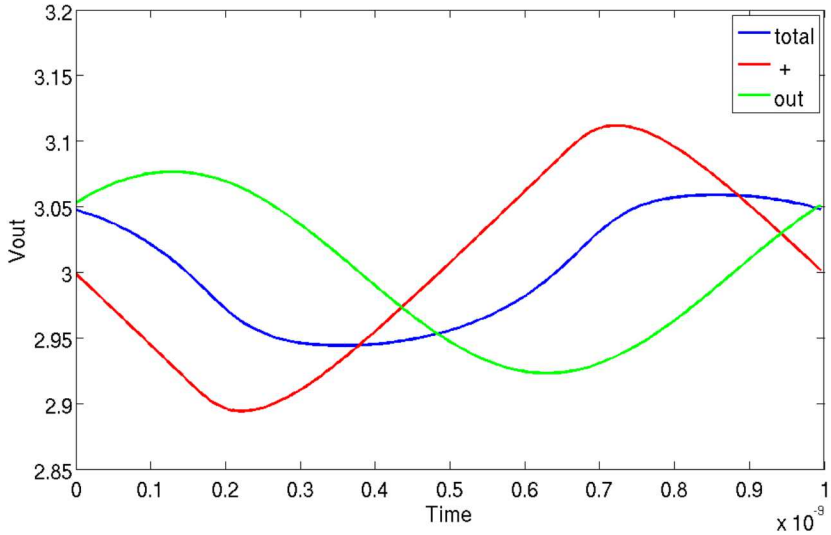

Figure 4-26. The effects from EM waves coupled to all traces

4.7. Practical High Bandwidth Op Amp

The LM6171 op amp is used in this example, which is a high-speed low-power low-distortion voltage feedback amplifier. It has a unity gain bandwidth product of 100 MHz and a very high slew rate of 3600 V/μs. The frequency response is shown in figure 4-27. The op amp PCB is excited by a 100 MHz plane wave. Therefore, EM disturbances are close to the working bandwidth.

In the first example, the EM wave is coupled to the non-inverting input trace and then is conducted to the input pin of the op amp. The induced voltage at the non-inverting input and the effect at the output is shown in figure 4-28. The peak to peak voltage at input is about 6.1 V. The in-band EM leads to a sinusoidal signal at the output due to very high slew rate.

The output voltage due to the EM disturbance on all traces is shown in figure 4-29. All traces are excited by a 100 MHz plane wave from the direction $\theta = 30°$ and $\phi = 60°$. As can be seen, the EM effect is a low distortion high frequency AC signal at the output.

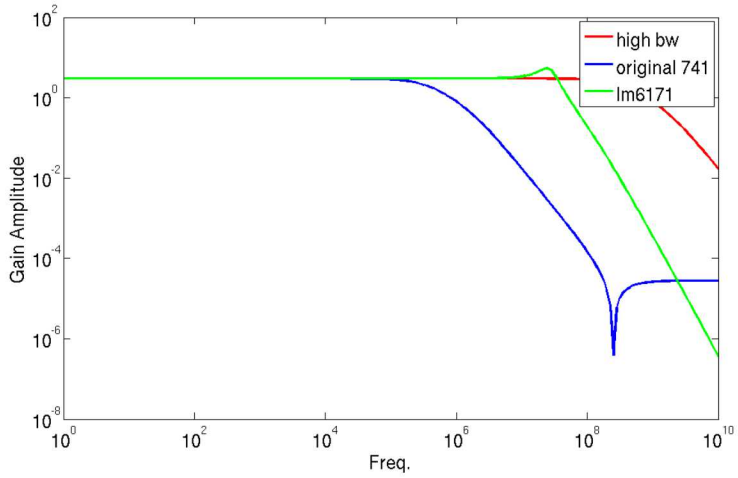

Figure 4-27. Frequency response of LM6171 op amp

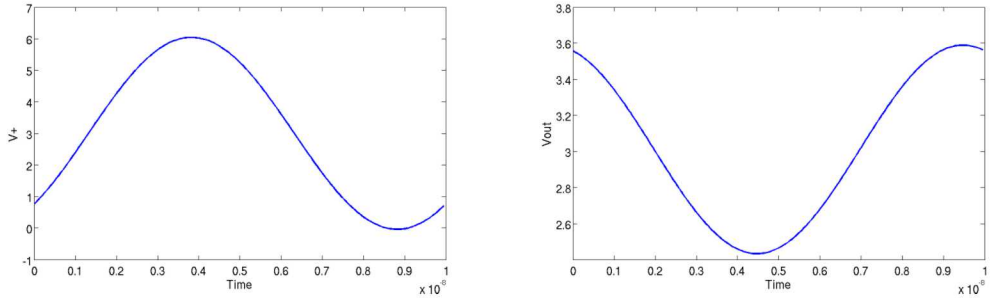

Figure 4-28. The induced voltage at the non-inverting input and the effect at the output

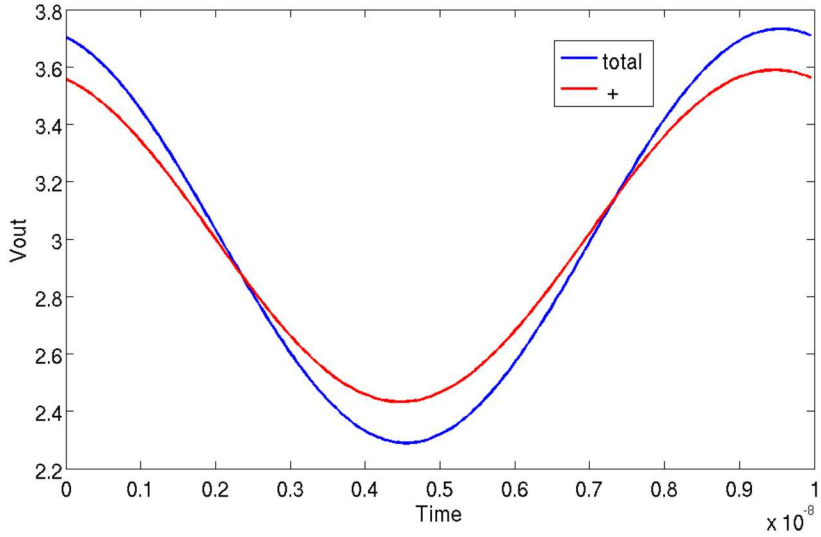

Figure 4-29. The effects from EM waves coupled to all traces

5. CONCLUSION

In this report, a robust and efficient approach to couple circuit and EM simulations has been established. To enable the coupling, a new and general frequency domain macromodel is developed in Xyce. A two step approach is established to calculate the required N port data from EIGER. The coupled simulation is achieved by using the Xyce HB simulation capability, which is extended to include a linear frequency domain macromodel.

The capability is tested for simple problems with linear and nonlinear loads, as well as practical op amp ICs exposed to incident plane waves. The approach is verified by multiple approaches. For linear circuits, the Xyce result is compared against EIGER results with an included load, and analytic solutions. For nonlinear circuits, verification is achieved by comparing against Hspice RF and a convergence study. The practical applications of the capability is demonstrated using multiple op amp circuits exposed to EM environments. A variety of situations are considered, including out-of-band and in-band EM disturbances, limited vs. high bandwidth and slew rate. These lead to various EM effects: DC shift, AC, low and high distortion, and combinations.

The coupled simulation capability enables the prediction of circuit response to EM environments. It not only improves our understanding EM effects on circuit performance for ND mission, but also provides guidance in design phase to improve EM performance. In addition, the work has established procedures and requirements for developing similar capabilities and provides future development directions.

REFERENCES

[1] *OrCAD PSpice*. https://www.orcad.com/products/orcad-pspice-designer/overview.

[2] J. Booth, S. Rajamanickam, and H. Thornquist. Basker: A threaded sparse lu factorization utilizing hierarchical parallelism and data layouts. In *Proceedings of the 2016 IEEE International Parallel and Distributed Processing Symposium Workshops (IPDPSW)*, pages 673–682. ACM, 2016.

[3] Leon O. Chua and Pen-Min Lin. *Computer-Aided Analysis of Electronic Circuits: Algorithms and Computational Techniques*. Prentice-Hall, Englewood Cliffs, New Jersey, 1975.

[4] W. Dong and P. Li. Hierarchical harmonic-balance methods for frequency-domain analog-circuit analysis. *IEEE Transactions on Computer-Aided Design of Integrated Circuits and Systems*, 26(12):2089–2101, 2007.

[5] P. Feldmann, B. Melville, and D. Long. Efficient frequency domain analysis of large nonlinear analog circuits. In *Proceedings of Custom Integrated Circuits Conference*, pages 461–464, 1996.

[6] G. Masetti, S. Graffi, D. Golzio, and Z. M. Kov´acs-V. Failures induced on analog integrated circuits by conveyed electromagnetic interferences: a review. *Microelectronics Reliability*, 36(7-8):955–972, 1996.

[7] G. Setti and N. Speciale. Design of a low EMI susceptibility CMOS transimpedance operational amplifier. *Microelectronics Reliability*, 38(6–8):1143–1148, 1998.

[8] I. Gil and R. Fern´andez-Garcia. Characterization and modelling of emi susceptibility in integrated circuits at high frequency. In *Proceedings of the IEEE International Symposium on Electromagnetic Compatibility (EMC EUROPE '12)*, pages 1–6, 2012.

[9] G.R. Boyle, B.M. Cohn, D. Pederson, and J.E. Solomon. Macromodeling of Integrated Circuit Operational Amplifiers. *IEEE Journal of Solid State Circuits*, SC-9(6):353–364, 1974.

[10] L. Han, X. Zhao, and Z. Feng. An efficient graph sparsification approach to scalable harmonic balance (HB) analysis of strongly nonlinear RF circuits. In *2013 IEEE/ACM International Conference on Computer-Aided Design (ICCAD)*, pages 494–499, 2013.

[11] C. W. Ho, A. E. Ruehli, and P. A. Brennan. The modified nodal approach to network analysis. *IEEE Trans. Circuits Systems*, 22(6):504–508, 1975.

[12] A. T. De Hoop. N-port receiving antenna and its equivalent electrical network. *Philips Res. Rep.*, 30:302–315, 1975.

[13] Eric R. Keiter, Thomas V. Russo, Richard L. Schiek, Heidi K. Thornquist, Ting Mei, Jason C. Verley, Peter E. Sholander, and Karthik V. Aadithya. Xyce Parallel Electronic Simulator: Users' Guide, Version 7.1. Technical Report SAND2020-5492, Sandia National Laboratories, Albuquerque, NM, 2020.

[14] Eric R. Keiter, Heidi K. Thornquist, Robert J. Hoekstra, Thomas V. Russo, Richard L. Schiek, and Eric L. Rankin. Parallel transistor-level circuit simulation. In Peng Li, Luís Miguel Silveira, and Peter Feldmann, editors, *Advanced Simulation and Verification of Electronic and Biological Systems*, chapter 1, pages 1–21. Springer, 2011.

[15] K.S. Kundert and A. Sangiovanni-Vincentelli. Simulation of nonlinear circuits in the frequency domain. *Computer-Aided Design of Integrated Circuits and Systems, IEEE Transactions on*, 5(4):521–535, October 1986.

[16] William L. Langston, Joseph Kotulski, Rebecca Coats, Roy Jorgenson, S. Adam Blake, Salvatore Campione, Aaron Pung, and Brian Zinser. Massively parallel frequency domain electromagnetic simulation codes. Technical Report SAND2018-0700C, Sandia National Laboratories, Albuquerque, NM, 2018.

[17] A. Mehrotra and A. Somani. A robust and efficient harmonic balance (hb) using direct solution of hb jacobian. In *2009 46th ACM/IEEE Design Automation Conference*, pages 370–375, 2009.

[18] R. C. Melville, P. Feldmann, and J. Roychowdhury. Efficient multi-tone distortion analysis of analog integrated circuits. In *Proceedings of the IEEE 1995 Custom Integrated Circuits Conference*, pages 241–244, 1995.

[19] M. Morgan and F. Tesche. Basic statistical concepts for analysis of random cable coupling problems. *IEEE Transactions on Antennas and Propagation*, 26(1):185–187, 1978.

[20] L. W. Nagel. SPICE 2, a computer program to simulate semiconductor circuits. Technical Report Memorandum ERL-M250, 1975.

[21] F. N. Najm. *Circuit Simulation*. John Wiley & Sons, Inc., 2010.

[22] Peng Li and L. T. Pileggi. Efficient harmonic balance simulation using multi-level frequency decomposition. In *IEEE/ACM International Conference on Computer Aided Design, 2004. ICCAD-2004.*, pages 677–682, 2004.

[23] V. Rizzoli, A. Costanzo, and G. Monti. General electromagnetic compatibility analysis for nonlinear microwave integrated circuits. In *Proc. IEEE MTT-S Int. Microw. Symp. Dig.*, volume 2, pages 953—956, June 2004.

[24] Heidi K. Thornquist, Eric R. Keiter, Robert J. Hoekstra, David M. Day, and Erik G. Boman. A parallel preconditioning strategy for efficient transistor-level circuit simulation. In *2009 IEEE/ACM International Conference on Computer-Aided Design - Digest of Technical Papers*, pages 410–417, 2009.

[25] Heidi K. Thornquist and Siva Rajamanickam. A hybrid approach for parallel transistor-level full chip circuit simulation. In M. Dayde, O. Marques, and K. Nakajima, editors, *High Performance Computing for Computational Science - VECPAR 2014*. Springer, 2014.

[26] F. Vanhee, D. Pissoort, J. Catrysse, G. A. E. Vandenbosch, and G. G. E. Gielen. Efficient reciprocity-based algorithm to predict worst case induced disturbances on multiconductor transmission lines due to incoming plane waves. *IEEE Transactions on Electromagnetic Compatibility*, 55(1):208–216, 2013.

[27] Jiri Vlach and Kishore Singhal. *Computer Methods for Circuit Analysis and Design*. Chapman & Hall, New York, 1994.

[28] Jeffery Williams, Larry Bacon, Michael Walker, and Erik Zeek. An Active THevenin Equivalent Network Approach to EMI/EMC problems. *IEEE International Symposium on Electromagnetic Compatibility*, 2014:878–881, September 2014.

[29] D. R. Wilton, W. A. Johnson, R. Jorgenson, R. Sharpe, and J. Rockway. EIGER: A new generation of computational electromagnetics tools. In *ElectroSft: Software for EE Analysis and Design*, pages 28–30, May 1996.

DISTRIBUTION

Email—Internal (encrypt for OUO)

Name	Org.	Sandia Email Address
Technical Library	01177	libref@sandia.gov

Sandia National Laboratories is a multimission laboratory managed and operated by National Technology & Engineering Solutions of Sandia LLC, a wholly owned subsidiary of Honeywell International Inc., for the U.S. Department of Energy's National Nuclear Security Administration under contract DE-NA0003525.